A Study of Segmentation and Normalization for Iris Recognition Systems

by

Ehsan M. Arvacheh

A thesis
presented to the University of Waterloo
in fulfillment of the
thesis requirement for the degree of
Master of Applied Science
in
Systems Design Engineering

Waterloo, Ontario, Canada, 2006

I hereby declare that I am the sole author of this thesis. This is a true copy of the thesis, including any required final revisions, as accepted by my examiners.

I understand that my thesis may be made electronically available to the public.

Ehsan M. Arvacheh

Abstract

Iris recognition systems capture an image from an individual's eye. The iris in the image is then segmented and normalized for feature extraction process. The performance of iris recognition systems highly depends on segmentation and normalization. For instance, even an effective feature extraction method would not be able to obtain useful information from an iris image that is not segmented or normalized properly. This thesis is to enhance the performance of segmentation and normalization processes in iris recognition systems to increase the overall accuracy.

The previous iris segmentation approaches assume that the boundary of pupil is a circle. However, according to our observation, circle cannot model this boundary accurately. To improve the quality of segmentation, a novel active contour is proposed to detect the irregular boundary of pupil. The method can successfully detect all the pupil boundaries in the CASIA database [42] and increase the recognition accuracy.

Most previous normalization approaches employ polar coordinate system to transform iris. Transforming iris into polar coordinates requires a reference point as the polar origin. Since pupil and limbus are generally non-concentric, there are two natural choices, pupil center and limbus center. However, their performance differences have not been investigated so far. We also propose a reference point, which is the virtual center of a pupil with radius equal to zero. We refer this point as the linearly-guessed center. The experiments demonstrate that the linearly-guessed center provides much better recognition accuracy.

In addition to evaluating the pupil and limbus centers and proposing a new reference point for normalization, we reformulate the normalization problem as a minimization problem. The advantage of this formulation is that it is not restricted by the circular assumption used in the reference point approaches. The experimental results demonstrate that the proposed method performs better than the reference point approaches.

In addition, previous normalization approaches are based on transforming iris texture into a fixed-size rectangular block. In fact, the shape and size of normalized iris have not been investigated in details. In this thesis, we study the size parameter of traditional approaches and propose a dynamic normalization scheme, which transforms an iris based on radii of pupil and limbus. The experimental results demonstrate that the dynamic normalization scheme performs better than the previous approaches.

Acknowledgements

I would like to express my gratitude to my supervisor, Prof. Hamid R.Tizhoosh. In the course of my master study, he has provided me with helpful ideas, guidance, comments and criticisms.

Many thanks to Adams Wai-Kin Kong, Ph.D. Candidate at University of Waterloo. We enjoyed research together. We discussed our ideas with the hope of getting closer to the truth. I thank him for all his help and encouragements during my master program.

Thank you to my readers, Prof. John S. Zelek and Prof. Kumaraswamy Ponnambalam for their useful comments on my thesis as well as their support during my time at University of Waterloo.

I would like to express my appreciation to the Chinese Academy of Sciences' Institute of Automation for generously providing the iris database.

I also thank Libor Masek for sharing his work as an open source iris recognition algorithm. I believe his algorithm is useful for researchers who start working in the field.

I sincerely thank Vicky Lawrence, the graduate secretary of Systems Design Department, for being helpful all the time.

Finally, I would like to thank my parents and my brother for believing in me and supporting me along the way. Thank you.

Contents

List of Figures

Chapter 1

Introduction

1.1 Biometric Technology

Biometric technology deals with recognizing the identity of individuals based on their unique physical or behavioral characteristics [13]. Physical characteristics such as fingerprint, palm print, hand geometry and iris patterns or behavioral characteristics such as typing pattern and hand-written signature present unique information about a person and can be used in authentication applications.

The developments in science and technology have made it possible to use biometrics in applications where it is required to establish or confirm the identity of individuals. Applications such as passenger control in airports, access control in restricted areas, border control, database access and financial services are some of the examples where the biometric technology has been applied for more reliable identification and verification.

In recent years, biometric identity cards and passports have been issued in some countries based on iris, fingerprint and face recognition technologies to improve border control process and simplify passenger travel at the airports. In UK and Australia, biometric passports based on face recognition are being issued [44]. The technology is designed to automatically take a picture from the passengers and match it to the digitized image stored in the biometric passports. Recently, US government is also conducting a Registered Traveler Program which uses a combination of fingerprint and iris recognition technology to speed up the security check process at some airports [45].

In the filed of financial services, biometric technology has shown a great potential in offering more comfort to customers while increasing their security. As an example, banking services and payments based on biometrics are going to be much safer, faster and easier than the existing methods based on credit and debit cards. Proposed forms of payments such as pay and touch scheme based on fingerprint or smart cards with stored iris information on them are examples of such applications. Although there are still some concerns about using biometrics in the mass consumer applications due to information protection issues, it is believed that the technology will find its way to be widely used in many different applications.

Moreover, access control applications such as database access and computer login also benefit from the new offered technologies. Compared to passwords, biometric technologies offer more secure and comfortable accessibility and have dealt with problems such as forgetting or hacking passwords. For instance, the new login method based on combination of a password with its typing pattern has been an innovative proposal where knowing the password itself would not be sufficient [4]. The method is based on typing pattern of a person by measuring the delays between the typing instances, which is a behavioral characteristic similar to hand written signature. The proposed method has added up the security of login-based access systems where a limited number of individuals are expected to have access to the systems.

Overall, the future of biometric technology is believed to be open for more investments based on the new services it has to offer to the society. A market overview, reported by the *International Biometric Group (IBG)*, indicates that the biometric industry revenue is expected to continuously rise from 1,538.9 million USD in 2005 to 5,749.2 million USD in 2010 [43]. Currently, this market revenue mostly relies on the existing fingerprint technologies; however, the new technologies based on face recognition, hand geometry and iris recognition are expected to relatively expand this revenue in near future.

1.2 Iris Recognition

Iris patterns are formed by combined layers of pigmented epithelial cells, muscles for controlling the pupil, stromal layer consisting of connective tissue, blood vessels and an anterior

border layer [1], [13]. The physiological complexity of the organ results in the random patterns in iris, which are statistically unique and suitable for biometric measurements [7]. In addition, iris patterns are stable over time and only minor changes happen to them throughout an individual's life [3]. It is also an internal organ, located behind the cornea and aqueous humor, and well protected from the external environment. The characteristics such as being protected from the environment and having more reliable stability over time, compared to other popular biometrics, have well justified the ongoing research and investments on iris recognition by various researchers and industries around the world. For instance, the developed algorithm by Daugman [7], which is known as the state-of-the-art in the field of iris recognition, has initiated huge investments on the technology for more than a decade. IriScan Inc. patents the core technology of the Daugman's system and several companies such as IBM, Iridian Technologies, IrisGuard Inc., Securimetrics Inc. and Panasonic are active in providing iris recognition products and services.

The history of iris recognition goes back to mid 19th-century when the French physician, Alphonse Bertillon, studied the use of eye color as an identifier [2]. However, it is believed that the main idea of using iris patterns for identification, the way we know it today, was first introduced by an eye surgeon, Frank Burch, in 1936 [6]. In 1987, two ophthalmologists, Flom and Safir, patented this idea [3] and proposed it to Daugman, a professor at Harvard University, to study the possibility of developing an iris recognition algorithm. After a few years of scientific experiments, Daugman proposed and developed a high confidence iris recognition system and published the results in 1993 [7]. The proposed system then evolved and achieved better performance in time by testing and optimizing it with respect to large iris databases.

The reports have shown that Daugman's system has zero false match rate based on the tests done by organizations such as British Telecom, US Sandia Labs, UK National Physical Laboratory, The National Biometric Test Center of SJSU, EyeTicket, Siemens, Unisys, LG, IriScan, Iridian, Sensar, and Sarno [9]. The information extracted from an iris is in binary format and it is stored in only 256 bytes to allow creation of nationwide IrisCode databases. The search engine is based on Boolean exclusive-OR operator (XOR) to allow extremely fast comparisons in the matching process. Moreover, the degrees-of-freedom of an IrisCode template, which indicates the statistical complexity of an iris based

on the entropy theory of Shannon [5], is about 249. The number of degrees-of-freedom of the iris templates shows that the complexity of iris patterns is relatively high compared to other biometric measures. The overall characteristics of the proposed algorithm offers real-time and high confidence identification in applications such as passenger control in airports, border control and access control in high-security areas. Currently, Daugman's iris recognition system is installed in several airports worldwide. Noteworthy to mention is the currently installed system in the United Arabs Emirates that is capable of identifying individuals within 2 seconds and performs about 2 billion comparisons daily.

A few years after the publication of the first algorithm by Daugman, other researchers developed new iris recognition algorithms. Systems presented by Wildes et al. [11], Boles and Boashash [14], Tisse et al. [16], Zhu et al. [17], Lim et al. [18], Noh et al. [19] and Ma et al. [20] are some of the well-known algorithms so far. Among these algorithms, the works done by Lim et al. and Noh et al. are also commercialized. The algorithms developed by Wildes and Boles are suitable for verification applications because the normalization of irises is performed in the matching process and would be very time consuming in identification applications. Although these algorithms have been successful, they still require to be improved in the accuracy and speed aspects compared to the proposed algorithm by Daugman.

Although Daugman's algorithm can perform fast and accurate recognition of irises, some details about the algorithm are not published. For instance, normalizing iris based on polar transformation requires a proper reference point as the polar origin. However, the details on this reference point have not been discussed. In this thesis, segmentation and normalization of iris is studied. The previous works on segmentation and normalization are evaluated and compared. Moreover, new segmentation and normalization methods are proposed that improve the recognition performance.

1.3 Thesis Objectives

The overall performance of an iris recognition system relies on the performance of its subsystems. The qualities of the image acquisition, segmentation, normalization and feature extraction, altogether, define the performance of the system. For instance, Lim reports

an 88.2% success rate over 6,000 iris images in the preprocessing stage due to undesired factors such as occlusion of irises by eyelids, shadow of eyelids and noises within pupils. Such degradation of the preprocessing stage could be considered as the degradation of the overall performance of the system.

1.3.1 Segmentation

Properly detecting the inner and outer boundaries of iris texture is significantly important in all iris recognition systems. All the previous segmentation techniques model iris boundaries and the two eyelids with simple geometric models. Pupil and limbus are often modeled as circles and the two eyelids are modeled as parabolic arcs. However, according to our observation, circle cannot model pupil boundary effectively. Irregular boundary of pupil is the motivation to create an accurate pupil detection algorithm based on the concept of active contours. The contour model takes into consideration that an actual pupil boundary is a near-circular contour rather than a perfect circle. The objective of this work is to demonstrate that this method can effectively improve the recognition accuracy.

1.3.2 Normalization

The next focus of this work is on iris normalization. Most normalization techniques are based on transforming iris into polar coordinates, known as unwrapping process. Pupil boundary and limbus boundary are generally two non-concentric contours. The non-concentric condition leads to different choices of reference points for transforming an iris into polar coordinates. Proper choice of reference point is very important where the radial and angular information would be defined with respect to this point.

In the experiments, first, the performance of several reference points are examined including pupil center, limbus center and the linearly-guessed center point. Unwrapping iris using pupil center is proposed by Lim [18] and Boles [15]. The linearly-guessed center is equivalent to the technique used by Joung [32]. The objective of the experiments is to illustrate the step-by-step improvements of the recognition results when the unwrapping reference point moves toward the linearly-guessed center point starting from the limbus center. Moreover, a contour-based unwrapping method is designed based on the assumption

that iris textures would not tend to be in excessive radial tension from pupil boundary to limbus boundary. This method reformulates the normalization problem as a minimization problem. The experimental results demonstrate that the proposed method performs better than the reference point approaches.

In addition, most normalization approaches based on Cartesian to polar transformation unwrap the iris texture into a fixed-size rectangular block. As an example, in Lim's method, after finding the center of pupil and the inner and outer boundaries of iris, the texture is transformed into polar coordinates with a fixed resolution. In the radial direction, the texture is normalized from the inner boundary to the outer boundary into 60 pixels. The angular resolution is also fixed to a 0.8° over the 360°, which produces 450 pixels in the angular direction. Other researchers such as Tisse et al., Boles et al. and Ma et al. also use the fixed size polar transformation model. This technique seems to be useful in bringing iris images into a standard form, which would simplify the feature extraction process. However, the circular shape of an iris implies that there are different number of pixels over each radius. Transforming information of different radii into same resolution results in different amount of interpolations, and sometimes loss of information, which may degrade the performance of the system. In this thesis, we investigate the size parameter of the fixed-size approach. Moreover, a new normalization technique is proposed which takes into account that iris textures have different number of pixels over each radius. The polar resolution of irises is then dynamically adjusted with respect to the number pixels in each radius. The experimental results demonstrate that the dynamic normalization scheme performs better than the fixed-size approach.

1.4 Thesis Layout

The rest of the thesis is organized as follows. Chapter 2 is background review of some well-known segmentation and normalization methods. In chapter 3, the proposed methods for improving segmentation and normalization are presented. Chapter 4 is the experimental results for illustrating the improvements of the proposed segmentation and normalization methods on the recognition performance. Chapter 5 offers concluding remarks and points out the contributions of this thesis.

Chapter 2

Background

2.1 Segmentation

In segmentation, it is desired to distinguish the iris texture from the rest of the image. An iris is normally segmented by detecting its inner (pupil) and outer (limbus) boundaries. Well-known methods such as the Integro-differential, Hough transform and active contour models have been successful techniques in detecting the boundaries. In the following, these methods are described and some of their weaknesses are pointed out.

2.1.1 Daugman's Integro-differential Operator

In order to localize an iris, Daugman proposed the Integro-differential operator [7]. The operator assumes that pupil and limbus are circular contours and performs as a circular edge detector. Detecting the upper and lower eyelids are also performed using the Integro-differential operator by adjusting the contour search from circular to a designed arcuate [9]. The Integro-differential is defined as:

$$\max(r, x_0, y_0) \left| G_\sigma(r) * \frac{\partial}{\partial r} \int_{(r,x_0,y_0)} \frac{I(x,y)}{2\pi r} ds \right|. \tag{2.1}$$

The operator pixel-wise searches throughout the raw input image, $I(x, y)$, and obtains the blurred partial derivative of the integral over normalized circular contours in different

radii. The pupil and limbus boundaries are expected to maximize the contour integral derivative, where the intensity values over the circular borders would make a sudden change. $G_\sigma(r)$ is a smoothing function controlled by σ that smoothes the image intensity for a more precise search.

2.1.2 Hough Transform

Hough transform is a standard image analysis tool for finding curves that can be defined in a parametrical form such as lines, polynomials and circles. The recognition of a global pattern is achieved using the local patterns. For instance, recognition of a circle can be achieved by considering the strong edges in an image as the local patterns and searching for the maximum value of a circular Hough transform.

Wildes et al. [13], Kong and Zhang [30], Tisse et al. [16] and Ma et al. [20] use Hough transform to localize irises. The localization method, similar to Daugman's method, is also based on the first derivative of the image. In the proposed method by Wildes, an edge map of the image is first obtained by thresholding the magnitude of the image intensity gradient:

$$| \bigtriangledown G(x,y) * I(x,y)|, \tag{2.2}$$

where $\bigtriangledown \equiv (\partial/\partial x, \partial/\partial y)$ and $G(x,y) = \frac{1}{2\pi\sigma^2} e^{-\frac{(x-x_0)^2+(y-y_0)^2}{2\sigma^2}}$. $G(x,y)$ is a Gaussian smoothing function with scaling parameter σ to select the proper scale of edge analysis.

The edge map is then used in a voting process to maximize the defined Hough transform for the desired contour. Considering the obtained edge points as (x_j, y_j), $j = 1, 2, ..., n$, a Hough transform can be written as:

$$H(x_c, y_c, r) = \sum_{j=1}^{n} h(x_j, y_j, x_c, y_c, r), \tag{2.3}$$

where

$$h(x_j, y_j, x_c, y_c, r) = \begin{cases} 1 & \text{if } g(x_j, y_j, x_c, y_c, r) = 0; \\ 0 & otherwise. \end{cases} \tag{2.4}$$

The limbus and pupil are both modeled as circles and the parametric function g is defined as:

$$g(x_j, y_j, x_c, y_c, r) = (x_j - x_c)^2 + (y_j - y_c)^2 - r^2. \tag{2.5}$$

Assuming a circle with the center (x_c, y_c) and radius r, the edge points that are located over the circle result in a zero value of the function. The value of g is then transformed to 1 by the h function, which represents the local pattern of the contour. The local patterns are then used in a voting procedure using the Hough transform, H, in order to locate the proper pupil and limbus boundaries. In order to detect limbus, only vertical edge information is used. The upper and lower parts, which have the horizontal edge information, are usually covered by the two eyelids. The horizontal edge information is used for detecting the upper and lower eyelids, which are modeled as parabolic arcs.

2.1.3 Discrete Circular Active Contours

Ritter proposed an active contour model to localize iris in an image [36]. The model detects pupil and limbus by activating and controlling the active contour using two defined forces: internal and external forces. The internal forces are responsible to expand the contour into a perfect polygon with a radius δ larger than the contour average radius. The internal force, $F_{int,i}$, applied to each vertex, V_i, is defined as:

$$F_{int,i} = \bar{V}_i - V_i, \tag{2.6}$$

where $\bar{V}_i$ is the expected position of the vertex in the perfect polygon. The position of $\bar{V}_i$ can be obtained with respect to C_r, the average radius of the current contour, and the contour center, $C = (C_x, C_y)$. The center of a contour is defined as:

$$C = (x_C, y_C) = \frac{1}{n} \sum_{i=1}^{n} V_i, \tag{2.7}$$

which is the average position of all contour vertices. The average radius of the contour is defined as:

$$C_r = \frac{1}{n}\sum_{i=1}^{n} \|V_i - C\|, \tag{2.8}$$

which is the average distance of all the vertices from the defined center point. The position of the vertices of the expected perfect polygon is then obtained as:

$$\bar{V}_i = (C_x + (C_r + \delta)cos(2\pi i/n), C_y + (C_r + \delta)sin(2\pi i/n)), \tag{2.9}$$

where n is the total number of vertices.

The internal forces are designed to expand the contour and keep it circular. The force model assumes that pupil and limbus are globally circular, rather than locally, to minimize the undesired deformations due to specular reflections and dark patches near the pupil boundary.

The contour detection process of the model is based on the equilibrium of the defined internal forces with the external forces. The external forces are obtained from the grey level intensity values of the image and are designed to push the vertices inward. The magnitude of the external forces is defined as:

$$\|F_{ext,i}\| = I(V_i) - I(V_i + \hat{F}_{ext,i}), \tag{2.10}$$

where $I(V_i)$ is the grey level value of the nearest neighbor to V_i. $\hat{F}_{ext,i}$ is the direction of the external force for each vertex and it is defined as a unit vector given by:

$$\hat{F}_{ext,i} = \frac{C - V_i}{\|C - V_i\|}. \tag{2.11}$$

Therefore, the external force over each vertex can be written as:

$$F_{ext,i} = \|F_{ext,i}\|\hat{F}_{ext,i}. \tag{2.12}$$

The movement of the contour is based on the composition of the internal and external forces over the contour vertices. Replacement of each vertex is obtained iteratively by:

$$V_i(t+1) = V_i(t) + \beta F_{int,i} + (1-\beta)F_{ext,i}, \tag{2.13}$$

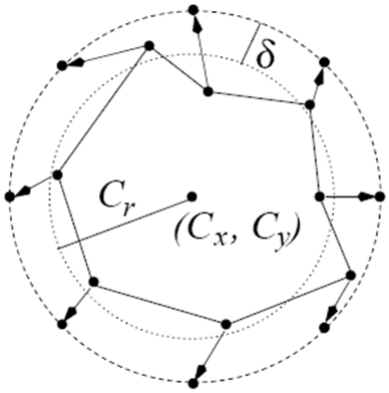

Figure 2.1: The internal forces of the Discrete Circular Active Contour

where β is a defined weight that controls the pace of the contour movement and sets the equilibrium condition of internal and external forces. The final equilibrium is achieved when the average radius and center of the contour becomes the same as the one in m iterations ago.

2.1.4 Other Segmentation Methods

Other researchers use methods similar to the described segmentation methods. For instance, the iris localization proposed by Tisse et al. is a combination of the Integro-differential and the Hough transform. The Hough transform is used for a quick guess of the pupil center and then the Integro-differential is used to accurately locate pupil and limbus using a smaller search space [16].

Lim et al. localize pupil and limbus by providing an edge map of the intensity values of the image. The center of pupil is then chosen using a bisection method that passes perpendicular lines from every two points on the edge map. The center point is then obtained by voting the point that has the largest number of line crossovers. The pupil and limbus boundaries are then selected by increasing the radius of a virtual circle with the

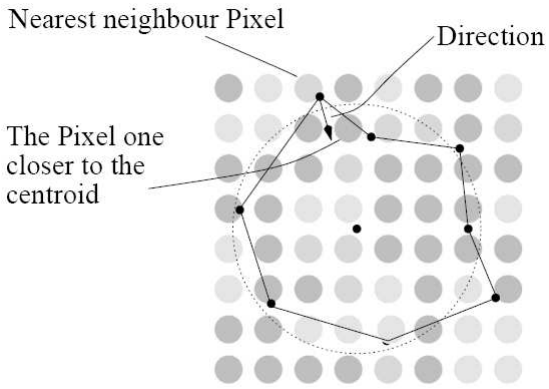

Figure 2.2: The external forces of the Discrete Circular Active Contour

selected center point and choosing the two radii that have the maximum number of edge crosses by the virtual circle as the pupil and limbus radii [18].

2.1.5 Problem Statement

The presented methods on locating the pupil and limbus assume that the boundaries are perfect circles. Although the approaches are different, all these methods consider pupil and limbus as circular curves. It has been noticed that the circular assumption of the contours can lead to inappropriate boundary detection. In figures 2.3 and 2.4, some of the iris images from the CASIA database are shown that the pupil boundaries are not perfect circles.

In addition, in the near-infrared images provided by the Institute of Automation, Chinese Academy of Sciences (CASIA), the limbus boundaries have insufficient contrast and global search techniques such as the Integro-differential operator are more suitable for the extraction process. However, even the global methods can result in false detection due to noises such as strong boundaries of upper and lower eyelids. The strong eyelid boundaries and presence of eyelashes affect the limbus localization significantly.

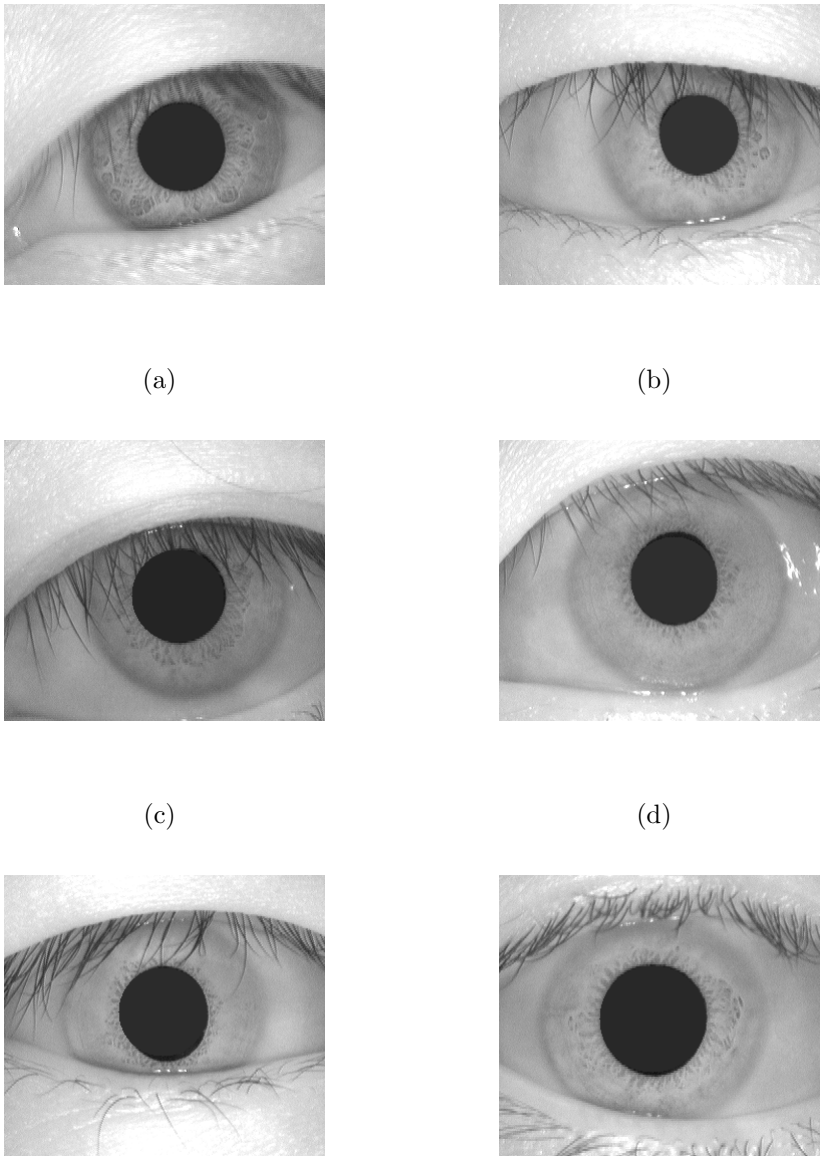

(a) (b)

(c) (d)

(e) (f)

Figure 2.3: (a)-(f) illustrate pupils that are not perfect circles.

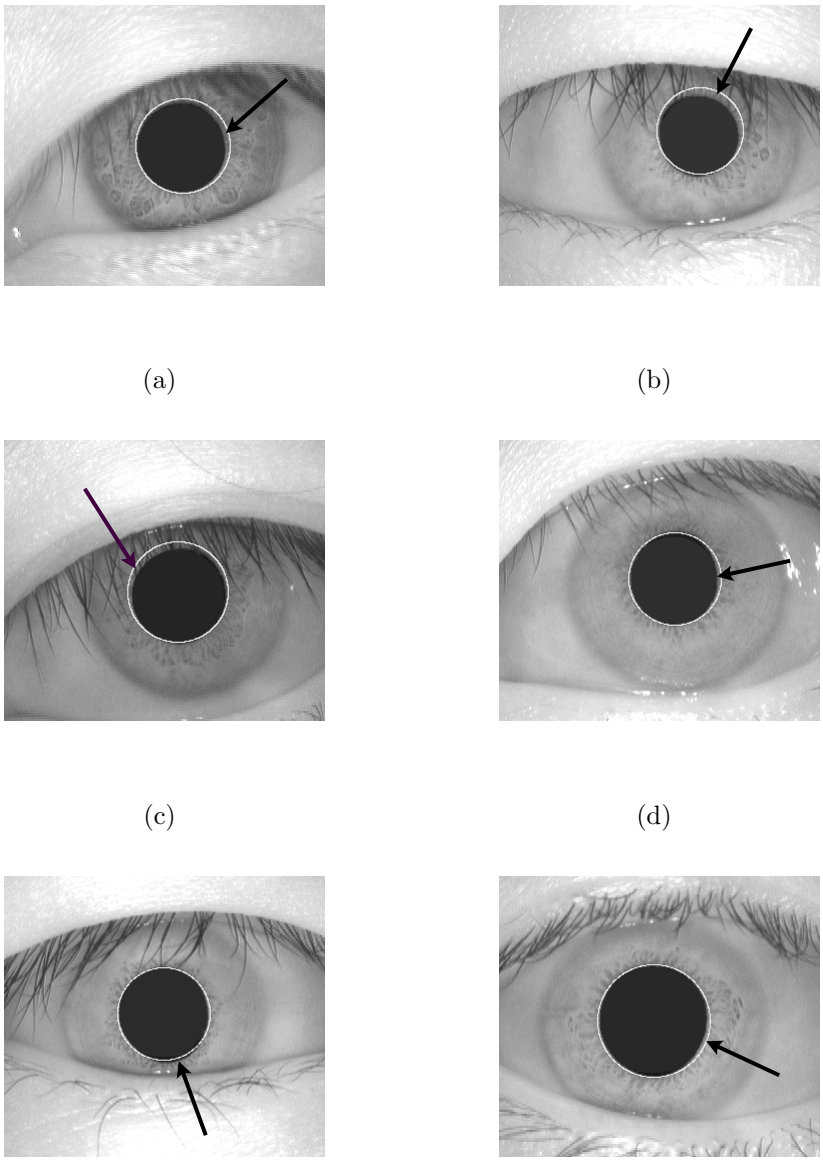

(a) (b)

(c) (d)

(e) (f)

Figure 2.4: (a)-(f) illustrate the results of the Integro-differential operator over the pupils that are not perfect circles. The circular contour does not detect pupil boundaries accurately.

Figure 2.5 shows some of the cases where the presence of eyelids and eyelashes have affected the localization process.

2.2 Normalization

Normalization refers to preparing a segmented iris image for the feature extraction process. In Cartesian coordinates, iris images are highly affected by their distance and angular position with respect to the camera. Moreover, illumination has a direct impact on pupil size and causes non-linear variations of the iris patterns. A proper normalization technique is expected to transform the iris image to compensate these variations.

2.2.1 Daugman's Cartesian to Polar Transform

Daugman's normalization method transforms a localized iris texture from Cartesian to polar coordinates. The proposed method is capable of compensating the unwanted variations due to distance of eye from camera (scale) and its position with respect to the camera (translation). The Cartesian to polar transform is defined as:

$$x(\rho,\theta) = (1-\rho) \times x_p(\theta) + \rho \times x_i(\theta),$$
$$y(\rho,\theta) = (1-\rho) \times y_p(\theta) + \rho \times y_i(\theta),$$

where

$$x_p(\theta) = x_{p0}(\theta) + r_p \times \cos(\theta),$$
$$y_p(\theta) = y_{p0}(\theta) + r_p \times \sin(\theta),$$
$$x_i(\theta) = x_{i0}(\theta) + r_i \times \cos(\theta),$$
$$y_i(\theta) = y_{i0}(\theta) + r_i \times \sin(\theta).$$

The process is inherently dimensionless in the angular direction. In the radial direction, the texture is assumed to change linearly, which is known as the rubber sheet model. The rubber sheet model linearly maps the iris texture in the radial direction from pupil border to limbus border into the interval [0 1] and creates a dimensionless transformation in the radial direction as well.

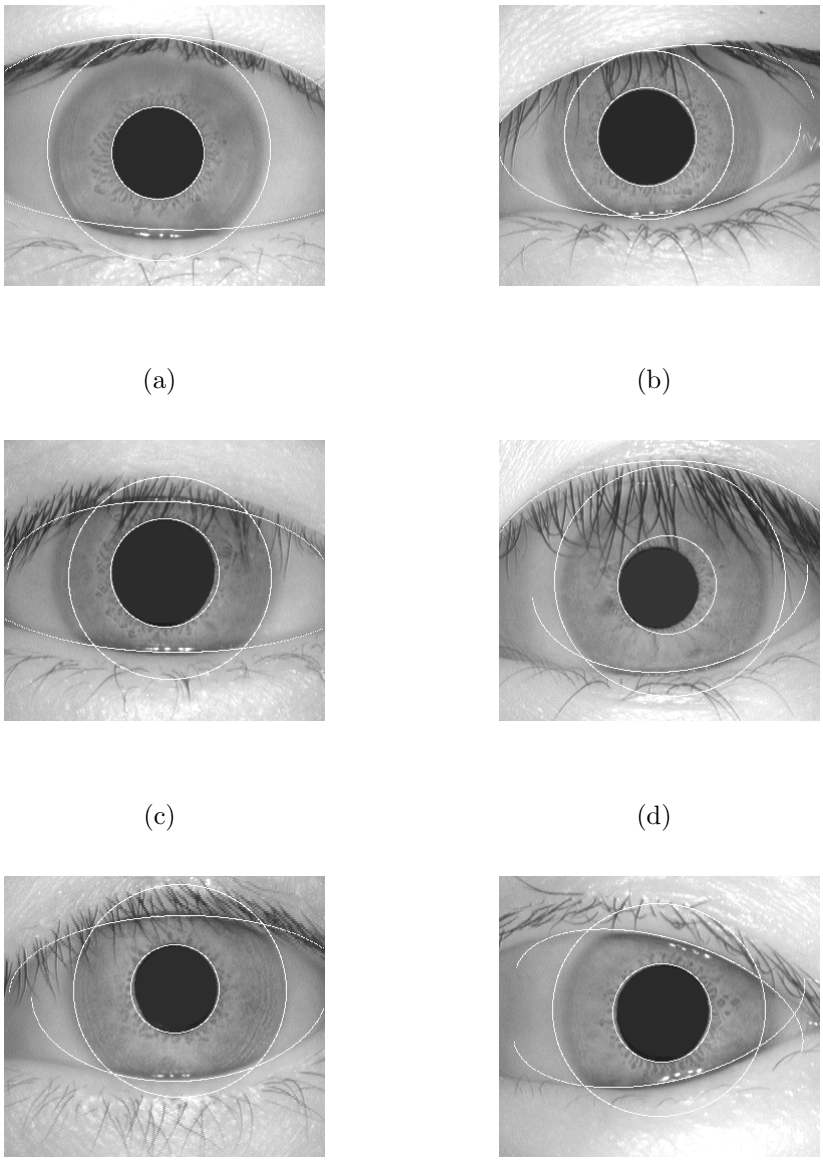

(a) (b)

(c) (d)

(e) (f)

Figure 2.5: (a)-(f) illustrate the inaccurate results of limbus detection because of low contrast of limbus and presence of eyelids and eyelashes.

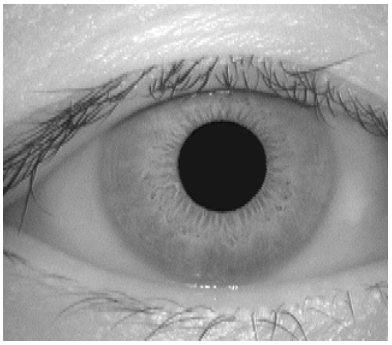

Figure 2.6: An iris image from CASIA database

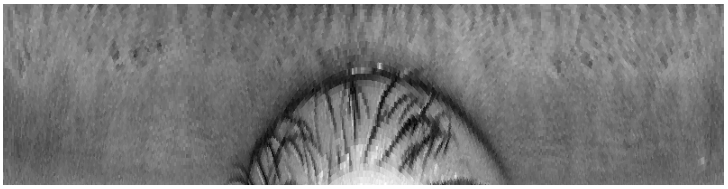

Figure 2.7: The normalized iris image using the Cartesian to polar transformation

Figure 2.6 illustrates an iris image in the Cartesian coordinates and its transformation result is illustrated in figure 2.7.

Although the normalization method compensates variations due to scale, translation and pupil dilation, it is not inherently invariant to the rotation of iris. Rotation of an iris in the Cartesian coordinates is equivalent to a shift in the polar coordinates. In order to compensate the rotation of iris textures, a best of n test of agreement technique is proposed by Daugman in the matching process. In this method, iris templates are shifted and compared in n different directions to compensate the rotational effects.

2.2.2 Wildes' Image Registration

Wildes has proposed an image registration technique for normalizing iris textures. In this method, a newly acquired image, $I_a(u, v)$ would be aligned with an image in the database, $I_d(u, v)$, that the comparison is performed. The alignment process is a transformation using a choice of mapping function, $(U(x, y), V(x, y))$ that would minimize the function:

$$\int_x\int_y (I_d(x, y) - I_a(x - u, y - v))^2 dxdy. \tag{2.14}$$

The alignment process compensates the rotation and scale variations. The mapping function is constrained to capture a similarity transformation of image coordinates (x, y) to $(x\prime, y\prime)$,i.e.,

$$\begin{pmatrix} \acute{x} \\ \acute{y} \end{pmatrix} = \begin{pmatrix} x \\ y \end{pmatrix} - \mathbf{sR}(\phi) \begin{pmatrix} x \\ y \end{pmatrix}, \tag{2.15}$$

with s as the scaling factor and $R(\phi)$ a matrix representing rotation by ϕ. The parameters s and ϕ are recovered by an iterative minimization procedure [41].

Wildes normalization process is based on a different approach compared to Daugman's method. In this method, normalization is performed in the matching time. Comparing to Daugman's approach, the normalization method would be time consuming in identification applications. However, for verification purposes the method is capable of compensating unwanted factors such as variations in rotation and scale.

2.2.3 Non-linear Normalization Model

The unwrapping method proposed by Daugman assumes that iris patterns are linearly distributed in the radial direction, which allows the mapping procedure into the interval [0 1]. The technique relies on two main factors:

1. The image acquisition process adjusts the pupil size to a proper radius range by adjusting the illumination.

2. The feature extraction process is locally applied to many different positions of the iris texture, which would compensate the local nonlinear variations.

The proposed non-linear normalization method proposed by Yuan and Shi [33], considers a nonlinear behavior of iris patterns due to changes of pupil size. In order to unwrap an iris region properly, a non-linear model and a linear normalization model are combined. The non-linear method, which is first applied to an iris image, is based on three assumptions:

1. The pupil margin and iris root (which correspond to the inner and outer boundaries of the iris) are concentric circles.

2. The margin of the pupil does not rotate significantly during pupil size changes.

3. The pupil shape does not change and remain circular when pupil size changes.

The non-linear model is defined by virtual arcs, which are named "fibers" following Wyatts work, that connect a point on the pupil border to a point on the limbus [34]. The polar angle traversed by the arcs between these two points is $\Pi/2$. The virtual arcs are defined based on normalized pupil sizes to a fixed value using a pre-defined λ_{ref}, which is obtained by the mean of all λ values defined as $\lambda = r/R$ in the iris database. The r and R represent the radius of pupil and limbus respectively. The reference annular zone with λ_{ref} is then linearly mapped into a fixed-size rectangle zone of $m \times n$ by equally sampling m points in each virtual concentric sampling circle with a fixed radial resolution.

It is concluded by the authors of the presented approach that the non-linear model still simplifies the real physiological mechanism of iris deformation and some more assumptions and approximations are required to support the model. The model is also believed to explicitly show the non-linear behavior of iris textures due to the improvements obtained in the experiments.

2.2.4 Other Normalization Methods

Lim et al. uses a method very similar to the pseudo polar transform of Daugman. In this method, after finding the center of pupil and the inner and outer boundaries of iris, the texture is transformed into polar coordinates with a fixed resolution. In the radial direction, the texture is normalized from the inner boundary to the outer boundary into

60 pixels which is fixed throughout all iris images. The angular resolution is also fixed to a 0.8 degree over the 360 degree which produces 450 pixels in the angular direction.

Boles' normalization technique is also similar to Daugman's method with the difference that it is performed at the time of matching. The method is based on the diameter of the two matching irises. The ratio of the diameters are calculated and the diameter of irises are adjusted to have the same diameters. The number of samples is also fixed and it is set to a power-of-two integer in order to be suitable for the dyadic wavelet transform.

In addition, there has been some research on the pseudo polar transform in order to optimize its performance. The work presented by Joung et al. [32] discusses the different possibilities of iris transformation. The research focuses on the fact that pupil and limbus are not always concentric and presents a method to improve the unwrapping process [32].

2.2.5 Problem Statement

Most of the normalization methods used in the proposed algorithms transform iris images from Cartesian to polar coordinates. This technique is efficient in the sense that the normalization process is performed prior to the matching time and is suitable for identification applications.

Although the normalization process proposed by Daugman has shown to be efficient, there are some aspects that are required to be investigated and discussed in details. The proposed pseudo polar transform is known to map an iris texture into the interval [0 1] in the radial direction . Moreover, in the original formulation of the transformation, each point over the iris texture is presented by a polar coordinate (r, θ). However, the question arises by the fact that pupil and limbus are not always concentric and the definition of polar coordinates requires a center point as the polar origin.

Some works such as the algorithms presented by Boles or Lim et al. unwrap the texture based on pupil center. A more recent research presented by Joung et al. uses an unwrapping method that improves the alignment of irises [32]. In this method, it is suggested to use limbus center to define the polar coordinates of the points over the limbus boundary and to use pupil center to define the polar coordinates of the pupil boundary. The coordinates of the other points between the two borders are then obtained linearly in the radial direction.

In addition, most normalization methods based on the Cartesian to polar transforma-

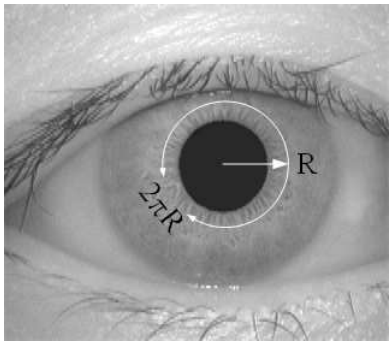

Figure 2.8: In each radius of iris there are different number of pixels.

tion unwrap iris textures into fixed-size rectangular blocks. The proposed technique seems to be useful in bringing iris images into a standard fixed resolution, which would simplify the feature extraction process. However, the circular shape of an iris implies that in each radius there are different number of pixels. Transforming information of different radii into a fixed-size block causes different interpolations, and sometimes loss of information, which may degrade the overall performance. Figure 2.8 illustrates that each iris radius represents a different perimeter that contains different number of pixels. In our experiments, the focus is to show enough evidence that although the presented methods are useful in normalization of irises, however, they may not be the optimal methods.

2.3 Summary

In this chapter, we have presented a summary of the previous segmentation approaches including Daugman's Integro-differential, Hough transform and the discrete circular active contour and of the previous normalization approaches including Daugman's Cartesian to polar transform, Wildes' image registration and non-linear normalization model. We also have pointed out some of their weaknesses that potentially degrade the performance. In the next chapter, we will propose methods to alleviate the effect of weaknesses.

Chapter 3

Proposed Methods

3.1 Segmentation

3.1.1 Pupil Detection: Proposed Near-circular Active Contour

In order to effectively extract a pupil boundary, it is essential to define the contour characteristics that the system aims to capture. In general, a pupil boundary is a closed, continuous and smooth curve, which is near-circular. In order to achieve a better performance in the next stages of an iris recognition system, it is essential to capture this contour with respect to a proper center point and a proper angular resolution. The center point of the contour is defined as the mean of the vertices, which can be written as:

$$C = (x_C, y_C) = \frac{1}{N} \sum_{i=1}^{N} V_i, \tag{3.1}$$

where N is the total number of vertices and V_i is the i^{th} vertex.

The angular resolution of the contour is another important aspect that should be considered. The continuity criterion is defined based on the angular resolution rather than the distance between the vertices which is common in general active contour models [38]. This resolution is chosen based on the average radius of pupils in the database of eye images. Considering the average radius of 45 pixels, the perimeter of a circle has around 285 pixels. In this case, a resolution of 400 angles is chosen in order to obtain contours that

are pixel-wise continuous. The number of vertices is constant and each vertex represents a specific angle throughout the process. This condition can be considered as angular forces that bring the vertices in the right angular position with respect to the updated contour center.

Each vertex of a contour is represented by a vector, which has a specific radius and direction with respect to the center point. In order to obtain a smooth curve with a near-circular shape, the internal forces are applied in the radial direction in a way to make the neighboring vertices have the same radius value in a proper angular range, $\Delta\theta$. The magnitude of an internal force applied to a single vertex is defined as:

$$|F_{int,i}| = \frac{1}{N_{\Delta\theta}} \times \left(\sum_{\theta_k=\theta_i-\frac{\Delta\theta}{2}}^{\theta_k=\theta_i+\frac{\Delta\theta}{2}} R_{\theta_k} \right) - R_i, \tag{3.2}$$

where $\Delta\theta$ represents the angular range, $N_{\Delta\theta}$ represents the number of vertices in the defined angular range and R_i is the radius of vertex i. Figure 3.1 illustrates the defined internal force over a vertex. The internal forces are designed to push the vertices in order to have the same radius as the mean radius of the vertices in the defined angular range.

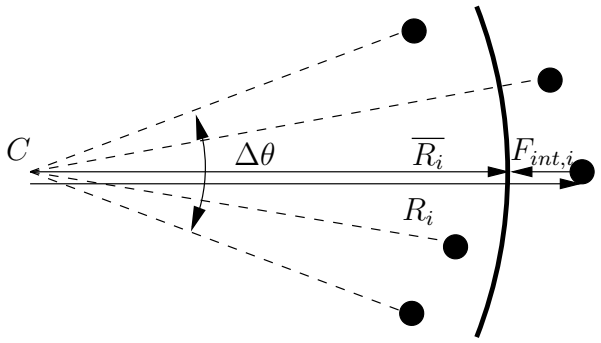

Figure 3.1: Internal force over a vertex. The internal force is designed to push the vertex to have the same radius as the mean radius of the vertices in the defined angular range.

The external forces are designed to pull the curve toward the maximum measured circular gradient and are applied in the radial direction as well. The circular gradient of an image around a center point is obtained by applying the Integro-differential operator in

different angles with the proper angular range, $\Delta\theta$. The Daugman's Integro-differential is basically a circular edge detector, which is defined as:

$$\underset{(r,x_0,y_0)}{\operatorname{argmax}} \left| G_\sigma(r) * \frac{\partial}{\partial r} \int_{(r,x_0,y_0)} \frac{I(x,y)}{2\pi r} ds \right|. \tag{3.3}$$

The original formulation of the Integro-differential integrates over the interval $[0, 2\pi]$, which is a complete circle. However, the definition of the external forces are based on obtaining the circular edge information in a smaller angular range. Our experiments show that an angular range of $\Delta\theta = \frac{\pi}{10}$ can be a proper value in order to obtain both the internal and external forces for the near-circular assumption of the pupil boundaries. The external forces are then defined by the radial distance of each vertex from the maximum circular gradient and can be written as:

$$|F_{ext,i}| = \underset{(R_C)}{\operatorname{argmax}} \left| \frac{\partial}{\partial r} \int_{\theta_i - \frac{\Delta\theta}{2}}^{\theta_i + \frac{\Delta\theta}{2}} \frac{I(x,y)}{2\pi r} ds \right| - R_i. \tag{3.4}$$

The proposed external forces which are based on gathering gradient information in the radial directions have the advantage that the contour would not stop in a local ridge or valley and the possibility of missing the pupil becomes very low. The search for the pupil boundary for obtaining the internal and external forces is performed by considering a search interval around the median value of the obtained radial information of pupil in the previous iteration. This technique increases the speed of the algorithm by limiting the search space and filters out the external forces that are pointing out to strong edges such as eyelids and eyelashes instead of the pupil boundary. In addition, in order to make the algorithm faster, the external forces are calculated in only 128 angular directions and the rest of the values would be interpolated based on the near-circular assumption of the pupil boundary in the angular range $\Delta\theta = \frac{\pi}{10}$.

The radial movement of the contour is based on composition of the internal and external forces over the contour vertices and the replacement of each vertex in the radial direction is obtained iteratively by:

$$R_{V_i}(n+1) = R_{V_i}(n) + F_{int,i} + \alpha \times F_{ext,i}, \tag{3.5}$$

where R_{V_i} is the radius of vertex i and $\alpha \in (0, 1)$ is a weight which controls the pace of contour movement and sets the equilibrium condition of internal and external forces. Smaller values of α result in smoother contours, however the contour moves toward the maximum gradient area in a slower pace. Increasing α increases the effect of external forces and the contour vertices move toward the pupil boundary in a faster pace. The value of α should be smaller than 1 to converge to the pupil boundary. If α is greater than 1, the contour would oscillate near the pupil boundary due to definition of the external forces. The final equilibrium is reached when the average radius and center of the contour become the same as the ones in the previous iteration.

In this process, there are fixed number of vertices. Each vertex represents a specific angle throughout the iterations with respect to the updated contour center. This condition can be considered as angular forces that are responsible for readjusting the angular position of the vertices with respect to the updated center point.

3.1.2 Eyelid Model: Elliptic Eyelid Contour

An eyelid contour model is derived from the assumption that an eyeball has a spherical shape. This assumption leads to an eyelid model based on the openness of the eye. The openness is defined as the angular position of an eyelid with respect to the center of the sphere. Assuming that an eyeball can be presented as a sphere:

$$x^2 + y^2 + z^2 = R^2_{eyeball}, \tag{3.6}$$

an eyelid curve can be obtained by intersecting this sphere with a plane which passes through the x axis with an angle ϕ with respect to the z axis. Figure 3.2 and 3.3 illustrate the side view and the front view of an eyelid contour considering the spherical shape of an eyeball and the expected eyelid curve in a specific degree of eye openness. This plane can be written as:

$$tan(\phi) = \frac{y}{z}. \tag{3.7}$$

The intersection curve simply becomes an elliptic curve:

$$x^2 + \frac{y^2}{sin(\phi)^2} = R^2_{eyeball}. \tag{3.8}$$

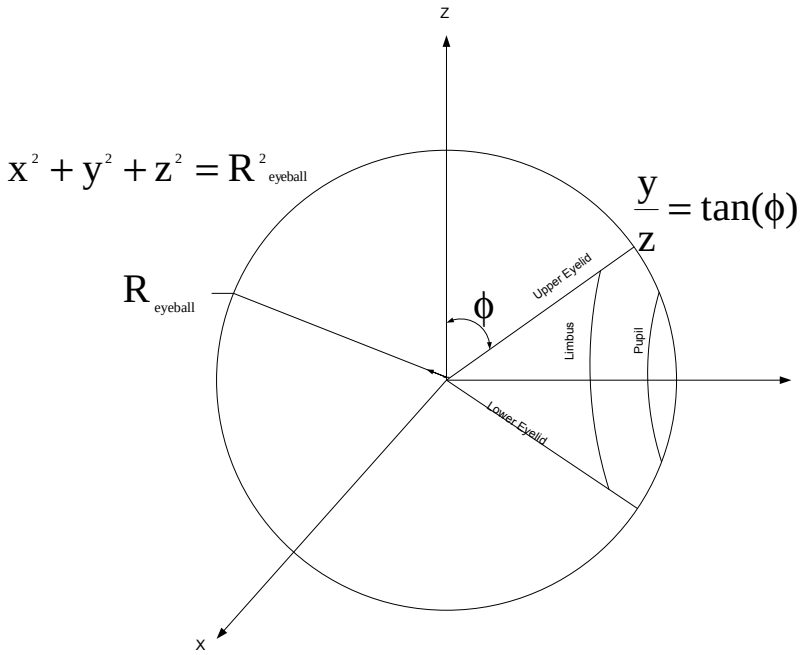

Figure 3.2: Eyelid curve model based on degree of eye openness: Side view.

This curve is then transformed to the polar coordinates to be more appropriate for our system:

$$x = rsin(\theta), y = rcos(\theta), \tag{3.9}$$

$$r = \frac{R_{eyeball}}{\sqrt{sin(\theta)^2 + \frac{cos(\theta)^2}{sin(\phi)^2}}}. \tag{3.10}$$

3.1.3 Limbus and Eyelids Detection: Iterative Algorithm

An iterative algorithm is developed in order to accurately locate limbus and eyelids boundaries. The extraction method uses the Integro-differential operator to detect the boundaries. The detection of an eyelid is based on the elliptic contours that are modeled by

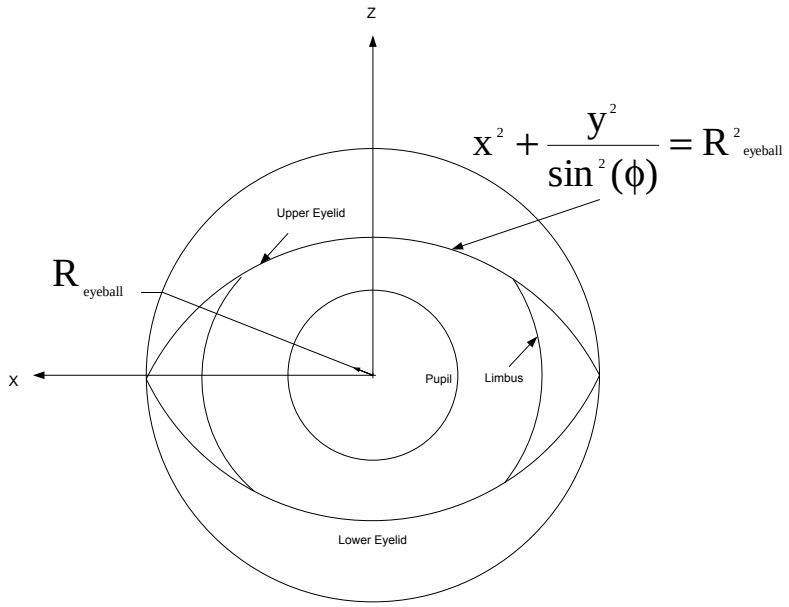

Figure 3.3: Eyelid curve model based on degree of eye openness: Front view.

the spherical shape of an eyeball and the expected eyelid curve in different degrees of eye openness.

In the near-infrared images provided by the Institute of Automation, Chinese Academy of Sciences (CASIA), the limbus boundaries have insufficient contrast and global search techniques such as the Integro-differential operator are more suitable for the extraction process. However, even the global methods can result in false detection because of noises such as strong boundaries of upper and lower eyelids.

The developed algorithm iteratively searches for iris and eyelids boundaries and excludes the detected eyelids areas for the next iteration. The process is designed with respect to the pupil center as the reference point and is performed by excluding the pixel values where the radius of limbus is larger than the radius of either upper or lower eyelids. This condition masks the areas where the iris is covered by the two eyelids and the process is repeated until the result of the search converges to a fixed center and radius for the limbus. Figure 3.4 illustrates the flowchart of the iterative algorithm.

3.1.4 Eyelash Detection: MAP Classification with Connectivity Criterion

Detecting eyelashes requires proper choice of features and classification procedure due to complexity and randomness of the patterns. The proposed eyelash detection by Kong et al. considers eyelashes as two groups of separable and multiple eyelashes and applies two different feature extraction methods to detect eyelashes [31]. A 1-D Gabor filter is applied to detect the separable eyelashes and an intensity variance is chosen for detecting the multiple ones. The two features combined with a connectivity criterion would lead to the decision of presence of eyelashes. In addition, an eyelash detection method is also proposed by Huang et al. that uses the edge information obtained by phase congruency of a bank of Log-Gabor filters. The edge information is also infused with the region information to localize the noise regions [29].

An eyelash detection algorithm is developed using the grey level intensities of the images combined with a connectivity criterion. The grey level intensity values are chosen as the

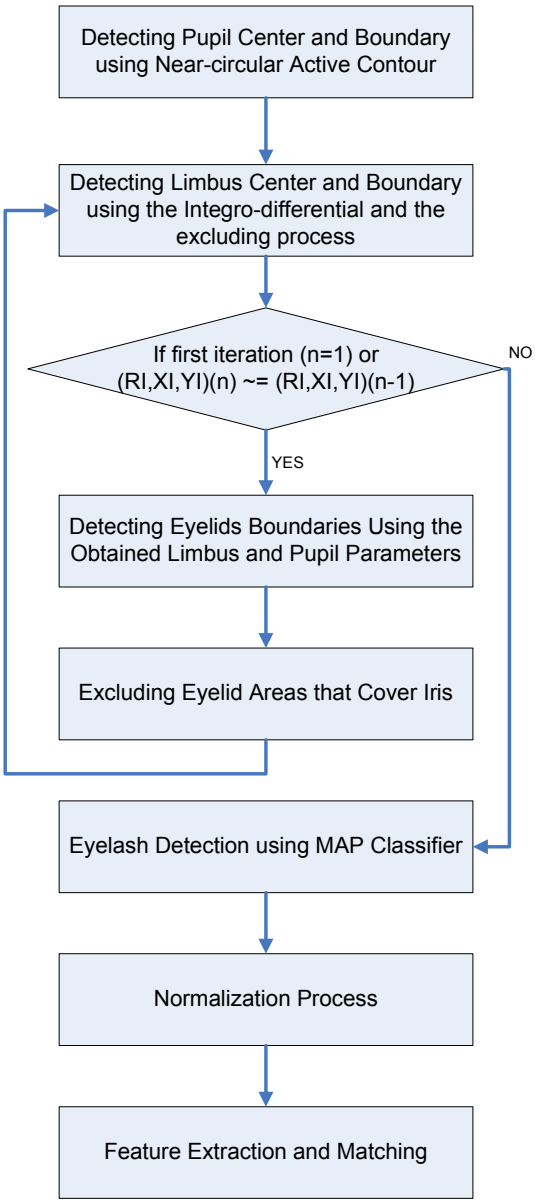

Figure 3.4: The iterative algorithm for limbus and eyelid detection.

features and the detection is based on a designed hierarchical MAP classification.

The MAP threshold is obtained by estimating the histogram of iris texture and the histogram of eyelashes. The histogram of iris and eyelashes are modeled as Gaussian distributions, which their mean and variance should be estimated. The histogram of an iris texture is estimated from the localized iris. However, eyelashes that cover the texture affect the histogram of the iris. In order to eliminate the effect of eyelashes, the maximum value of the obtained histogram is considered as the mean value of the iris texture. The variance is then estimated only from the values of the histogram that are greater than the mean in order to eliminate the effect of eyelashes covering the iris.

The mean and variance of the histogram of eyelashes is estimated in a similar way as the iris with the difference of considering the area outside the localized iris. In the images provided by the CASIA, pupil area and eyelashes have the lowest intensity values. Mean value of an iris is higher than the two areas and the mean value of the rest of the image is higher than the mean of the iris texture. Considering that the assumption is true for every image, the mean value of eyelashes is defined as the local maximum that occurs 2σ lower than the iris mean value. This definition of the mean value of eyelashes is based on a trial and error process to prevent obtaining values that represent the iris texture. The variance of the eyelashes is then estimated using only the values that are less than the estimated mean value assuming all the areas that are darker than the estimated mean value refer to the eyelashes in the image. The variance estimation technique is designed to eliminate the effect of noises in the histogram estimation process. Figure 3.5 illustrates the estimated iris and eyelash histograms and the MAP threshold.

The MAP threshold is obtained by the estimated histograms and eyelash detection is performed by a hierarchical classification using a connectivity criterion. The classification algorithm is a region growing process. The initial region of the iris texture is obtained by thresholding the localized image by the estimated mean value of the iris texture and applying the connectivity criterion. The largest connected area that the values are larger than the mean value is then chosen as the initial iris region. The initial region of the eyelashes is also determined by the same method. The largest connected area that the values are less than the mean value of eyelashes is chosen as the initial eyelash region. The region growing process is then designed based on thresholding the image and checking the

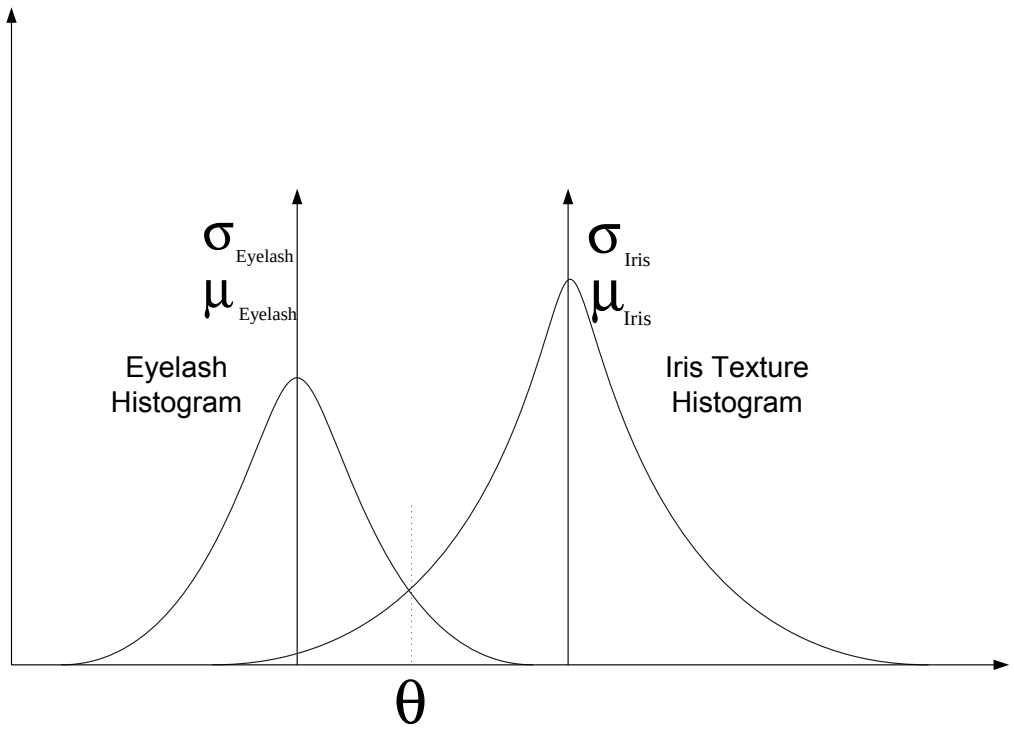

Figure 3.5: The estimated histogram of iris and eyelashes and the MAP threshold.

connectivity criterion in a way that the classification of the two regions would reach and pass the MAP threshold at the same.

3.2 Normalization

3.2.1 Iris Unwrapping: Proposed Contour-Based Model

Transforming iris texture from Cartesian to polar coordinates, known as the unwrapping process, is one of the stages of an iris recognition algorithm, and has a significant impact on the overall performance of the system.

The main purpose of an iris texture is to control the amount of light entering the eye in different illumination conditions. The studies on physiology of iris illustrates that the response of the texture with respect to different intensities of light is non-linear due to the distribution of iris muscles controlling the pupil size [27]. An iris texture consists of two main muscles that are distributed in the angular and radial directions, known as the sphincter and dilator muscles, respectively. In strong light conditions, in order to decrease the pupil diameter, the sphincter muscle contracts while the dilator muscle stays relaxed to adjust the light that enters the eye. However, in the conditions where the light is weak, the sphincter muscle relaxes and the dilator muscle contracts to increase the pupil diameter to allow more light to enter the eye.

The two different illumination conditions, strong light and weak light, which cause the iris texture to perform in two different modes result in a non-linear behavior of the iris texture. As an evidence of such behavior, the non-linear variations of the pupil center with respect to the limbus center, which is a fixed point, could be mentioned.

In the field of iris recognition, studying the behavior of irises seems to be essential to be able to propose a proper normalization technique. In order to describe the importance of a normalization method more thoroughly, it could be helpful to emphasize the uniqueness of each individual's iris and its stability over time as the bases of all iris recognition systems. Assuming that each iris has unique patterns that do not change over time, it is desired to capture these patterns every time an image is taken from the eye. However, an iris texture is highly sensitive to illumination and the texture deforms to change the pupil diameter

and control the amount of light entering the eye. The deformation of the texture also results in the deformation of the iris patterns. In other words, the iris patterns change due to different illumination conditions. In order to obtain the unique patterns of the iris, it is desired to be able to track the changes of the iris to recover the unique patterns.

It should be mentioned that the way an iris responses to illumination also varies from eye to eye due to different distributions of the muscles controlling the pupil. Therefore, it seems more practical to study the behavior of a large number of irises to obtain a normalization model that is optimal in capturing and tracking the patterns. In this thesis, different normalization methods are examined over irises in the CASIA database in order to find an optimal normalization technique.

Limbus Center: the Unwrapping Reference Point

The limbus center of an iris can be used as the reference point to unwrap the iris texture. The possible advantage of this point is that limbus contour is fixed and does not change over time. Figure 3.6 shows an unwrapping method using limbus center as the reference point.

Pupil Center: the Unwrapping Reference Point

Pupil center can also be considered as a proper choice for the reference point. Lim et al. and Boles et al. algorithms are both based on pupil center as the reference point. Unwrapping an iris with respect to this point seems to be advantageous in extracting features from the areas near the pupil, where the iris textures have more defined patterns, and may lead to acceptable recognition results. Figure 3.7 shows an unwrapping method using pupil center as the reference point.

Minimum Distance Unwrapping Method

An unwrapping method is examined based on the minimum distance of the points over the pupil boundary from the ones over the limbus boundary. In this method, N equally spaced points are chosen over the limbus boundary and the corresponding points over the pupil boundary have been selected based on the minimum distance criterion. The method

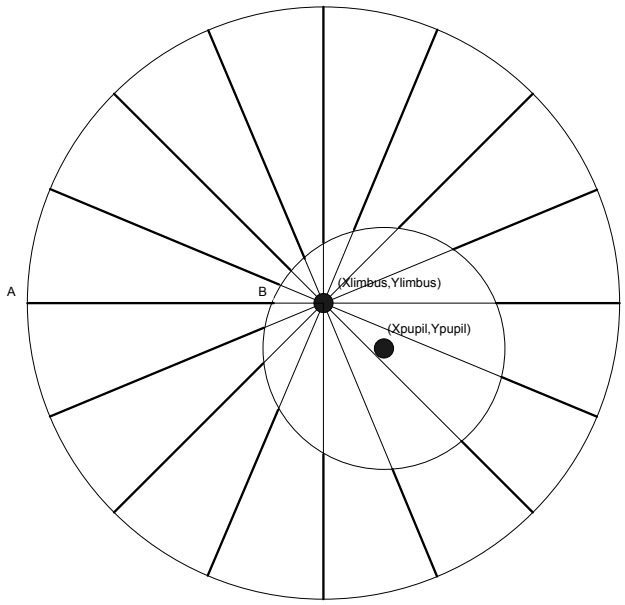

Figure 3.6: Unwrapping using the limbus center as the reference point.

results in global and local minimum distance between the points over the two boundaries. It should be noticed that the minimum distance method can cause irregular resolution over the pupil boundary due to different positioning of the pupil center with respect to limbus center.

In addition, the experiments have been repeated for the condition where N equally spaced points are chosen over the pupil boundary instead of the limbus boundary to consider their potential differences.

Contour-Based Method: Global Minimum

Similar to the minimum distance method, an unwrapping method is studied based on the global minimum of the distances between the limbus and pupil boundaries. In this method, spite of the minimum distance method, the points that are chosen over both of the borders are equally spaced and the positioning of the two borders are based on their global distance. The global minimum distance of the contour-based model is defined as:

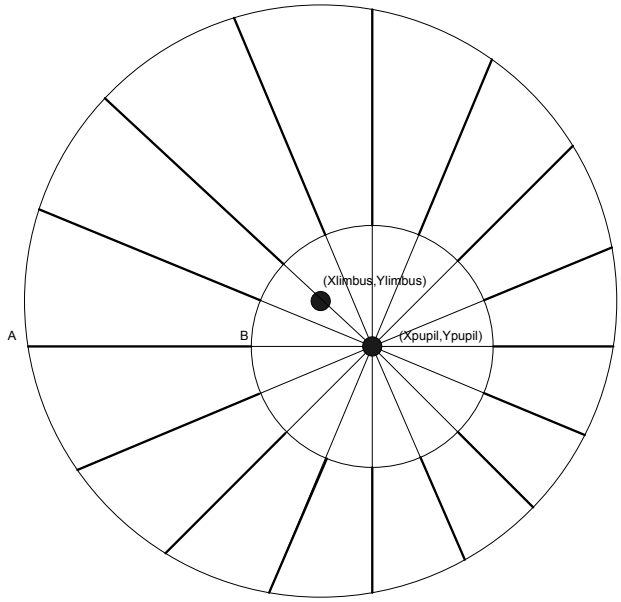

Figure 3.7: Unwrapping using the pupil center as the reference point.

$$\underset{(x_p(\theta_o),y_p(\theta_o))}{\operatorname{argmin}} \left(\int_0^{2\pi} \sqrt{((x_i - x_p(\theta))^2 + (y_i - y_p(\theta))^2)}d(\theta)\right), \tag{3.11}$$

where (x_i, y_i) and (x_p, y_p) are the limbus and pupil borders respectively. θ_o is defined as the angular offset for the pupil border in order to minimize the global minimum formulation.

The initial idea of both the minimum distance and the contour-based methods have arisen from the assumption that an iris texture tends to be in its most relaxed state in each pupil diameter. Therefore, it would make sense to adjust the points over the two borders in a way that the texture would not be in excessive radial tension. Moreover, both the minimum distance and the contour-based models have the advantage over the center based techniques in cases where the pupils are not perfectly circular. In cases where the pupil borders are not perfect circles and have been detected by the active contour model, center-based models may not be as robust as contour based models with due to the sensitivity of the normalization to the correct choice of center point.

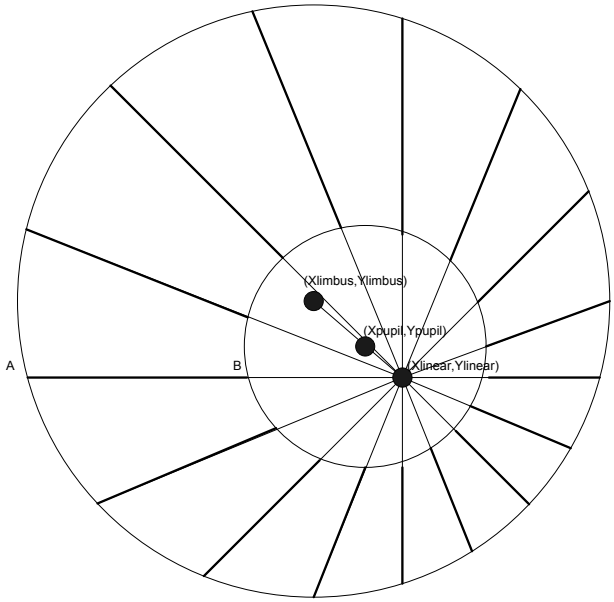

Figure 3.8: Unwrapping using the linearly-guessed center as the reference point.

Linearly-Guessed Reference Point Method

In addition to the center-based models based on limbus and pupil centers, the performance of a linearly-guessed center point is also examined. In this method, the reference point is obtained by a linear estimation using centers and radii of pupil and limbus. Figure 3.8 illustrates the method for positioning the reference point. This method suggests that the unwrapping process should be performed by a point that the pupil center tends to reach when the pupil radius approaches to zero. The limbus center and radius are considered as the starting state and the pupil center and radius are considered as a measurement in order to linearly guess the the position of the pupil center when its radius is zero.

It should be mentioned that the linearly-guessed center point is equivalent to the unwrapping method presented by Joung [32]. Figure 3.9 illustrates the equivalence of the linearly-guessed method with the method based on unwrapping an iris with respect to both limbus and pupil centers.

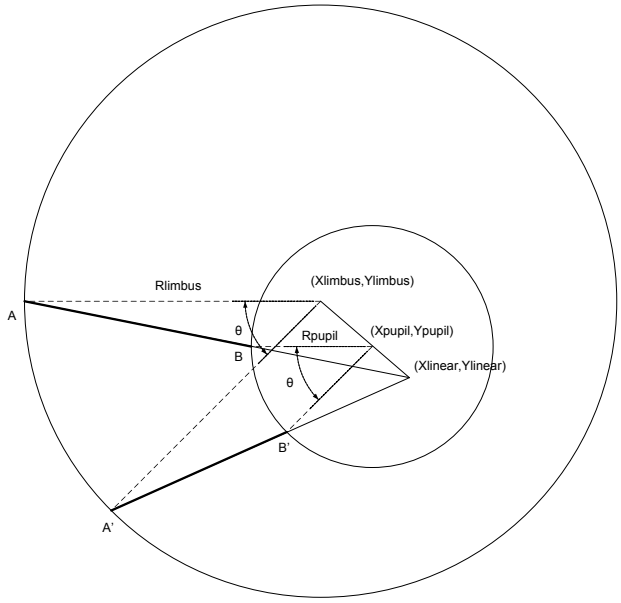

Figure 3.9: Double-reference method used by Joung is equivalent to the proposed linearly-guessed center point.

3.2.2 Iris Normalization: Proposed Dynamic-Size Model

In addition to the choice of the unwrapping method for transforming an iris image from Cartesian to polar coordinates, the concept of sampling frequency is also essential to be discussed in details. It should be noted that an iris image is in discrete form. As an example, the images provided by the CASIA database are 280×320, which can be considered as 280×320 samples from the area the image is taken. Daugman suggests capturing iris images with approximately 100 to 200 pixels in diameter and suggests that this resolution should not be less than 50 pixels over the iris diameter. However, the image acquisition proposed by Wildes suggests capturing around 256 pixels in diameter.

Considering that the number of samples obtained from an iris is finite and satisfies the mentioned minimum resolution criterion, another sampling issue arises at the time of transforming an iris from Cartesian to polar coordinates. The Cartesian to polar transformation is defined for the continuous form of images. However, in the discrete form, the transformation encounters two main problems:

1. The polar samples do not perfectly match the Cartesian samples, so the polar values are required to be estimated.

2. In each radius of the polar coordinates, there is different number of samples in the Cartesian coordinates, which can cause problems such as uncontrolled sampling, excessive interpolation and in some cases loss of information.

One of the most commonly used normalization methods is to transform an iris from Cartesian to polar coordinates with fixed radial and angular resolutions. The works presented in [18],[14] and [20] are based on a fixed-size transformation. However, as it has been described, the normalization process causes uncontrolled over-sampling, excessive interpolation and in some cases loss of information.

In this work, the proposed method takes into consideration that each radius of iris has different number of samples relative to the radius. The normalization technique transforms an iris image from Cartesian coordinates to polar coordinates with an angular resolution relative to the radius of the area where the features are extracted. Figure 3.11 is a graphical demonstration of the model with respect to 8 radial locations. In this method, angular

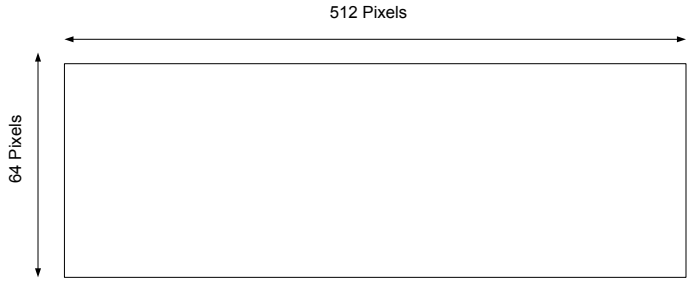

Figure 3.10: An example of a fixed-size normalization approach.

resolution is a linear factor of radius, which controls interpolation in each radial positioning and prevents loss of information.

3.3 Summary

In this chapter, we have presented several different methods including the near-circular active contour, the elliptic eyelid model, the iterative algorithm, the hierarchical eyelash detection for accurate segmentation. We also provide methods including the linearly-guessed reference point, the contour-based model and the dynamic-size technique for effective normalization. The experimental results will be offered in the coming chapter.

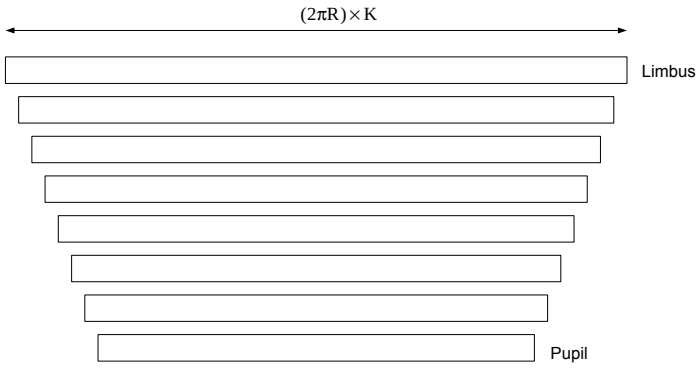

Figure 3.11: The proposed dynamic-size method. In this method, size of rectangular blocks are adjusted by perimeter of pupil and limbus boundaries.

Chapter 4

Experimental Results

4.1 Segmentation

4.1.1 Pupil Detection

The performance of the proposed active contour with respect to different values of α is illustrated in figures 4.1 and 4.2. Figure 4.1 shows that smaller values of α generate smoother contours and the vertices move toward pupil boundary in a slower pace. However, as it shown in figure 4.2, increasing the value of α, increases the effect of external forces and makes the contour vertices to move toward the pupil boundary in a faster pace. The value of α should be smaller than 1 in order to prevent the contour from oscillating around the pupil boundary due to the definition of the external forces. It should be mentioned that the initial center of contour is obtained by first thresholding the image to obtain the dark regions representing pupil and eyelash regions. In the CASIA database, the value of the threshold is set to 65 in grey level scale. The center of contour is then initialized as center of mass of the obtained dark regions.

In addition, the accuracy of the external and internal forces highly depends on the position of the contour center point. The contour center is the reference point for calculating the internal and external forces in the defined angular range $\Delta\theta = \frac{\pi}{10}$. As the contour center becomes closer to the pupil center, the internal and external forces are measured more accurately because of better adjustment of the angular arcs with respect to the pupil

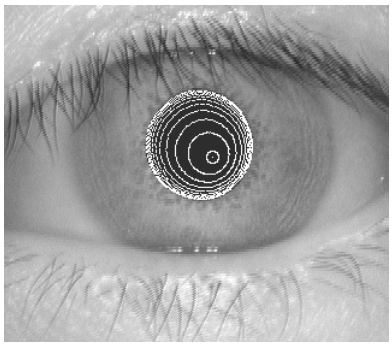

Figure 4.1: Near-circular active contour with $\alpha = 0.3$. Smaller values of α make the contour progression slower and increase its smoothness.

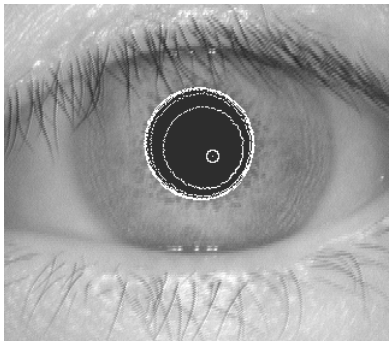

Figure 4.2: Near-circular active contour with $\alpha = 0.7$. Larger values of α make the contour progression faster and decrease its smoothness.

boundary. The external forces are designed to pull the curve toward the maximum circular gradient. The definition of the external forces makes the contour vertices to move in a way that the contour center gradually becomes closer to the actual pupil center. Therefore, calculation of the internal and external forces becomes more accurate after each iteration.

Figure 4.3 illustrates the results of pupil detection using the circular Integro-differential. It is shown that the actual pupil boundaries would not be properly located when the contours are assumed to be circular. The results of the near-circular active contour are shown in figure 4.4, where the location of pupil borders of figure 4.3 are detected accurately. In section 4.2.1, the recognition improvements of the active contour is demonstrated compared to the traditional circular pupil detection. The near-circular active contour has a 100% success rate and is able to accurately detect all the 756 iris images in the CASIA database.

4.1.2 Eyelid Model

The proposed elliptic eyelid model has shown a great potential in detecting the eyelid borders. The curve model is defined in the polar coordinates with respect to pupil center. The search for the eyelid contours is performed by the Integro-differential operator using the proposed curve model. The search space of the operator is defined based on the polar representation of equation 3.10 with respect to the pupil center over a range of values for the $R_{eyeball}$ and θ. The value of $R_{eyeball}$ varies from R_{limbus} to $2R_{limbus}$, where R_{limbus} is the estimated limbus radius in the previous iteration. The value of θ, which defines the orientation of the eyelid contour, is chosen to vary in the interval $[-\frac{\pi}{8}, \frac{\pi}{8}]$ to compensate the possible eye rotations. The fixed choice of angular resolution normalizes the eyelid contours, where an equal number of samples would be considered over each curve at the time the Integro-differential operator is applied.

Figure 4.5 illustrates some of the successful eyelid detections. The dark areas in the images are the iris textures that are covered by the eyelids which are excluded for the feature extraction and matching process.

This model has been able to accurately detect eyelids of 708 images out of the 756 images in the CASIA database. In addition, different cases of unsuccessful detection are studied. There are three main cases where the eyelids are not properly detected. Figure 4.6

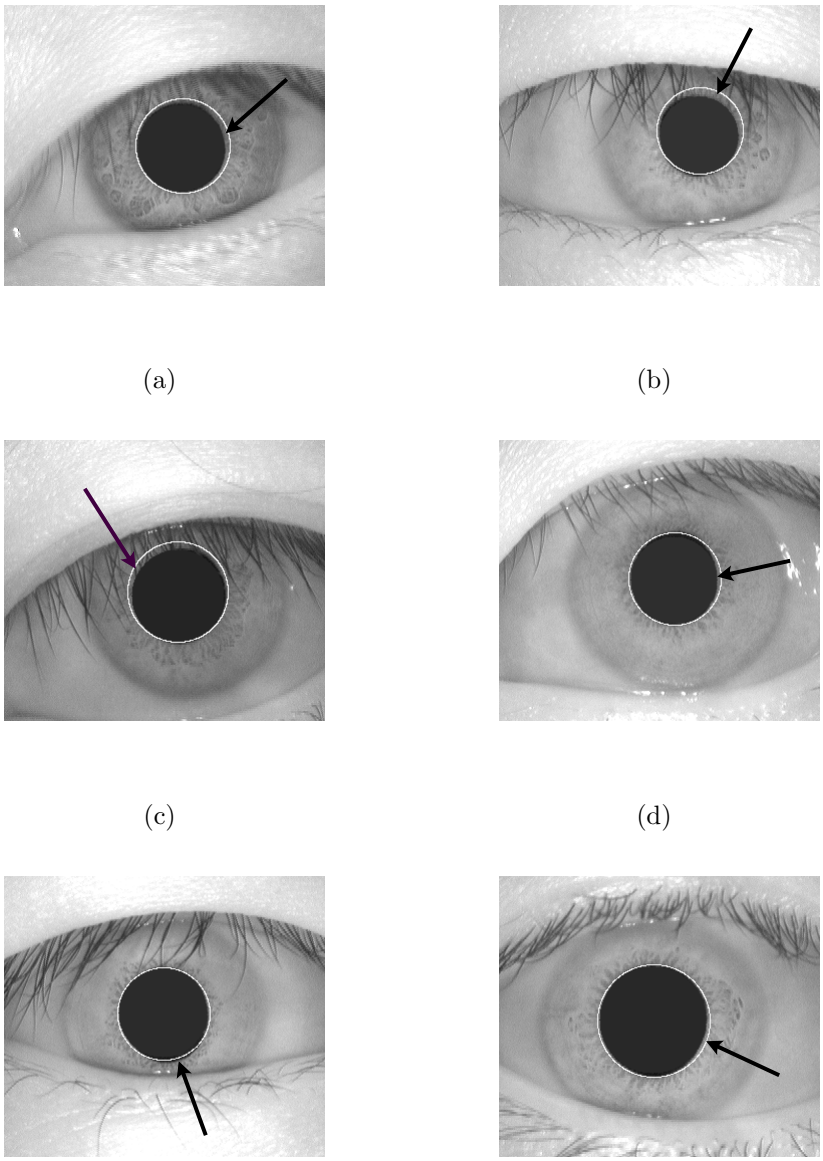

(a) (b)

(c) (d)

(e) (f)

Figure 4.3: (a)-(f) illustrate the results of pupil detection using the Integro-differential operator with circular contour. The arrows illustrate misalignments of the circles with the pupil boundaries. Circle cannot model pupil boundary accurately.

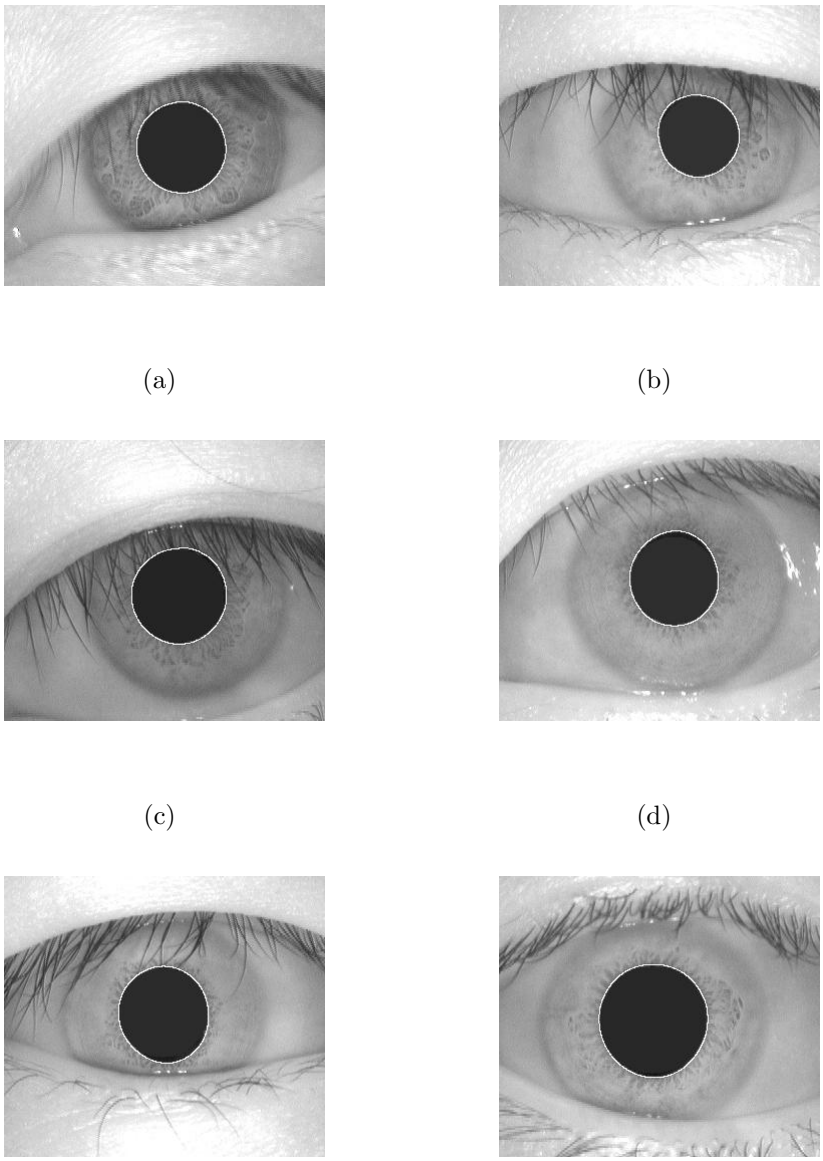

(a) (b)

(c) (d)

(e) (f)

Figure 4.4: (a)-(f) illustrate the results of the proposed active contour over the near-circular pupils. The active contour locate pupil boundaries more accurately compared to the results of the Integro-differential operator in figure 4.3.

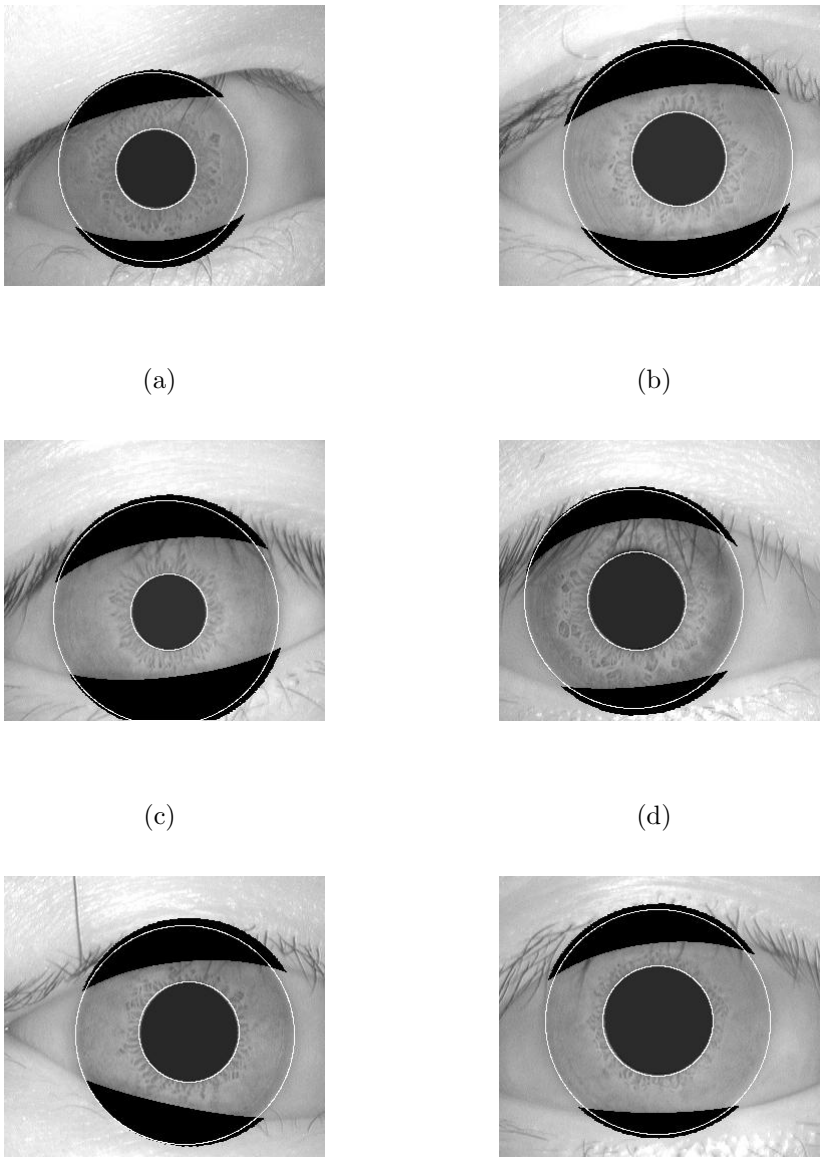

(a) (b)

(c) (d)

(e) (f)

Figure 4.5: (a)-(f) illustrate successful eyelid detection using the elliptical model. The algorithm excludes the iris regions that are covered by upper and lower eyelids. These regions are shown by the dark areas.

illustrates a case where eyelids are not detected properly due to a *double eyelid* condition. In this case, there are two contours over each eyelid and the algorithm detects the one with higher edge contrast. In addition, figure 4.7 illustrates another case where the eyelids are covered by eyelashes. In this case, the algorithm improperly detects noisy areas where eyelashes are present rather than the eyelid contours. Finally, figure 4.8 indicates a case where the position of eyelids are detected, however, the contour model is not in proper alignment with the actual eyelid contour. These misalignments are because of the range of parameters $R_{eyeball}$ and θ, which adjust the shape of the eyelid contours. However, increasing the range of these parameters would increase the time required for eyelid detection. Therefor, it is essential to define them to optimize both accuracy and speed of the system.

4.1.3 Limbus and Eyelids Detection

Figure 4.9 shows the results of the boundary detection based on the circular Integro-differential. As it is shown in the figure, strong edges of eyelids and presence of eyelashes can mislead the algorithm in detecting the location of limbus boundaries. The limbus boundaries of the CASIA database have insufficient contrast and detecting the boundaries requires less noisy search space. The proposed algorithm is designed to iteratively exclude areas of irises that are covered by eyelids to create less noisy search space to locate the limbus boundaries. The iterative algorithm is also capable of fast detection of the borders. Figure 4.10 shows the results of localization based on the proposed iterative algorithm that improves the limbus detection of figure 4.9. The localizations have been completed in only two iterations.

The iterative algorithm has improved the overall segmentation performance by improving both limbus detection and eyelid detection results. There have been 42 cases where the limbus boundaries were not detected properly and the iterative algorithm has been able to localize these boundaries. Moreover, the algorithm has been able to improve the eyelid detection of 8 iris images that the eyelids were not detected accurately.

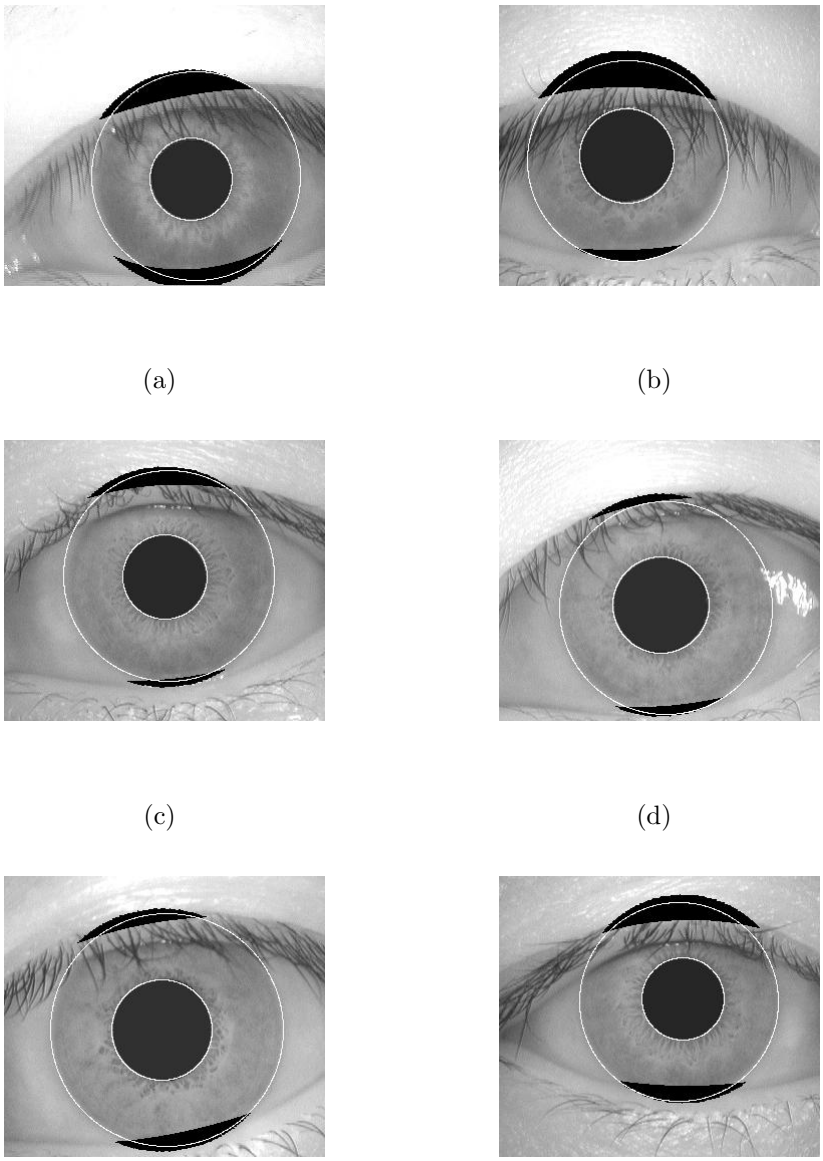

(a) (b)

(c) (d)

(e) (f)

Figure 4.6: (a)-(f) illustrate unsuccessful cases of eyelid detection due to the double eyelid condition. As it is shown in the images, some eyelids appear as two contours. However, the algorithm detects the contour with the higher edge contrast.

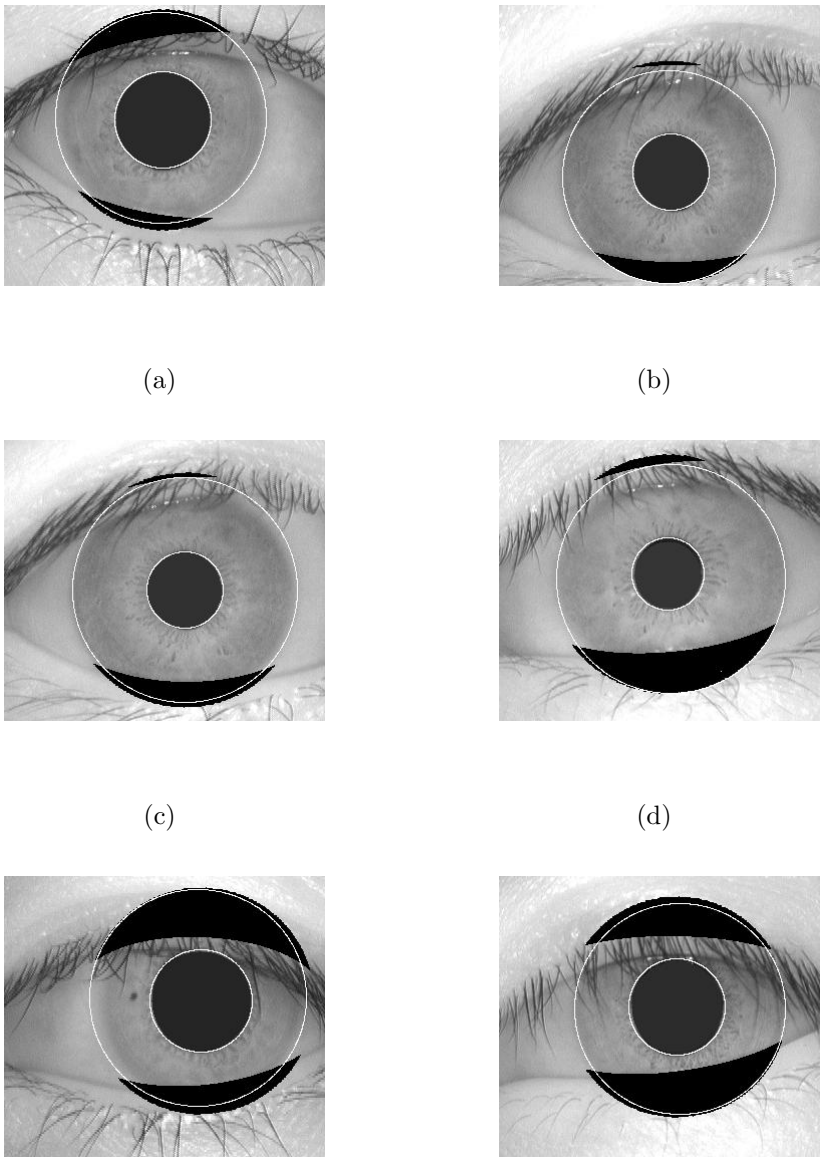

(a) (b)

(c) (d)

(e) (f)

Figure 4.7: (a)-(f) illustrate unsuccessful cases of eyelid detection due to excessive presence of eyelashes over the eyelid contours. In cases where eyelid contours are covered by eyelashes, the algorithm may not detect the eyelids.

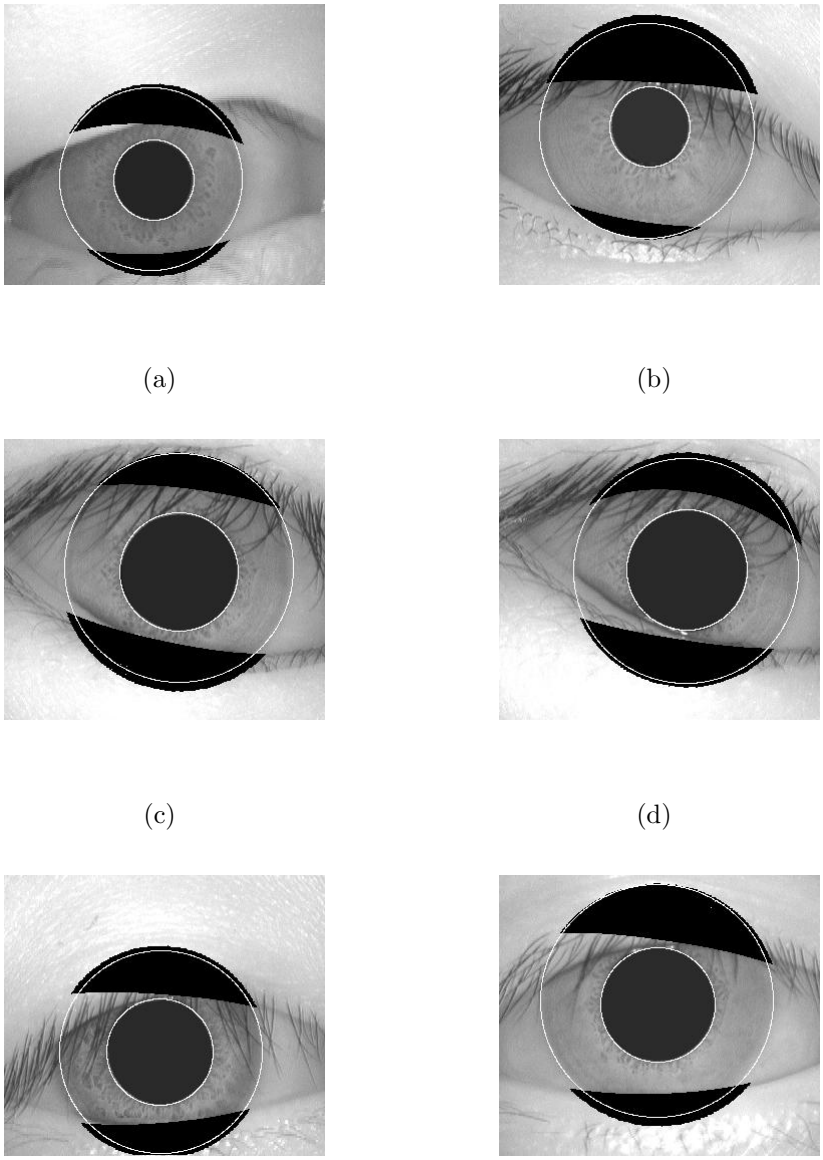

(a) (b)

(c) (d)

(e) (f)

Figure 4.8: (a)-(f) illustrate unsuccessful cases of eyelid detection due to misalignment of the eyelid model with the actual eyelid contours. The main reason of these misalignments is the range of parameters that control the shape of contours. However, increasing the range of parameters would increase the time required for eyelid detection.

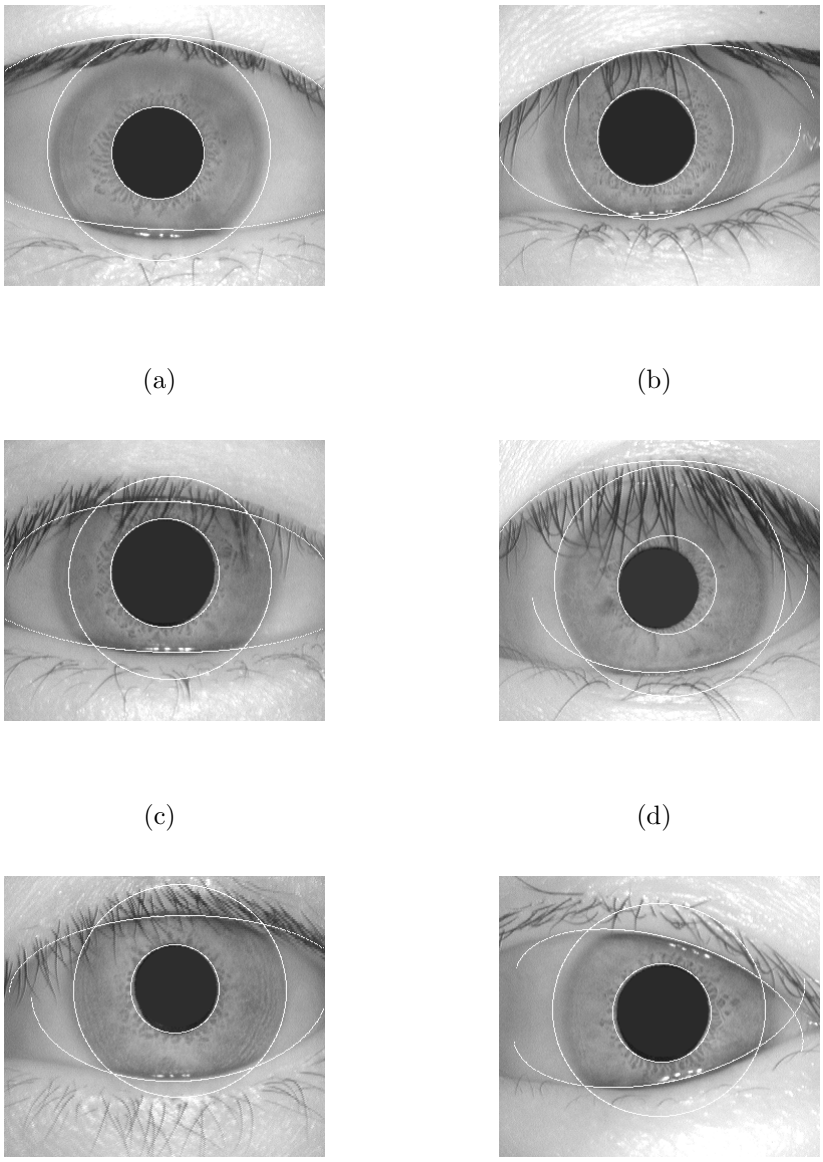

(a) (b)

(c) (d)

(e) (f)

Figure 4.9: (a)-(f) illustrate the inaccurate results of limbus detection because of low contrast of limbus and presence of eyelids and eyelashes.

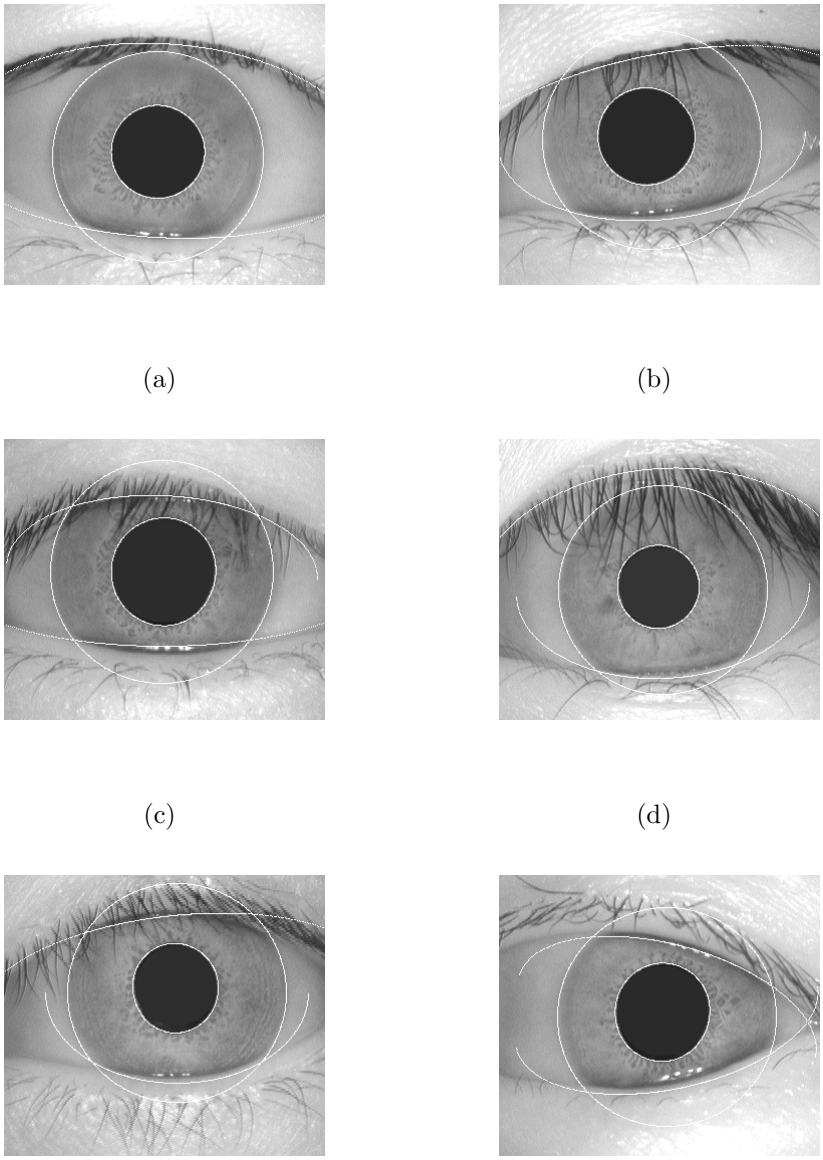

(a) (b)

(c) (d)

(e) (f)

Figure 4.10: (a)-(f) illustrate results of the iterative algorithm in improving the limbus detection process by eliminating the noisy areas. The limbus boundaries are accurately detected in 2 iterations.

4.1.4 Eyelash Detection

The proposed eyelash detection algorithm is based on thresholding the grey level intensity values of iris image. The grey level intensity value of the images is a suitable choice for feature because of its flexibility with respect to irregular eyelash patterns. Figure 4.11 illustrates some CASIA images and figure 4.12 illustrates the successfully detected eyelashes.

Although, the use of grey level intensity values has shown a great potential in eyelash detection and the algorithm has been successful in many images, there are some aspects that are essential to be pointed out. The developed algorithm highly depends on the quality of the estimated histograms, where several prior assumptions are taken into account. For instance, the mean of the histograms are estimated as the maximum values of the histograms, which may not be accurate enough. In addition, the histograms are assumed to be symmetric and the variances are estimated only from half of the values in the histogram. These basic assumptions can lead to improper estimation of the MAP threshold. Figure 4.13 illustrates some of the cases where the eyelashes are not properly detected due to incorrect MAP threshold.

The proposed algorithm has been successful in cases where the histograms and the MAP threshold have been estimated accurately. However, in order to develop more robust eyelash detection, it is essential to estimate the histograms more accurately.

The previous approaches for detecting eyelashes based on 1-D Gabor filter [31] or the phase congruency [29] are based on the edge information obtained from the images. These feature extraction methods are suitable for detecting separable eyelashes, which could be identified by their phase information. However, these methods would not be able to detect multiple eyelashes that have irregular patterns and the phase information would not represent useful information. In order to develop a more accurate and robust eyelash detection algorithm, it seems promising to combine the features based on phase information with the grey level intensity values to improve the performance of the eyelash detection process.

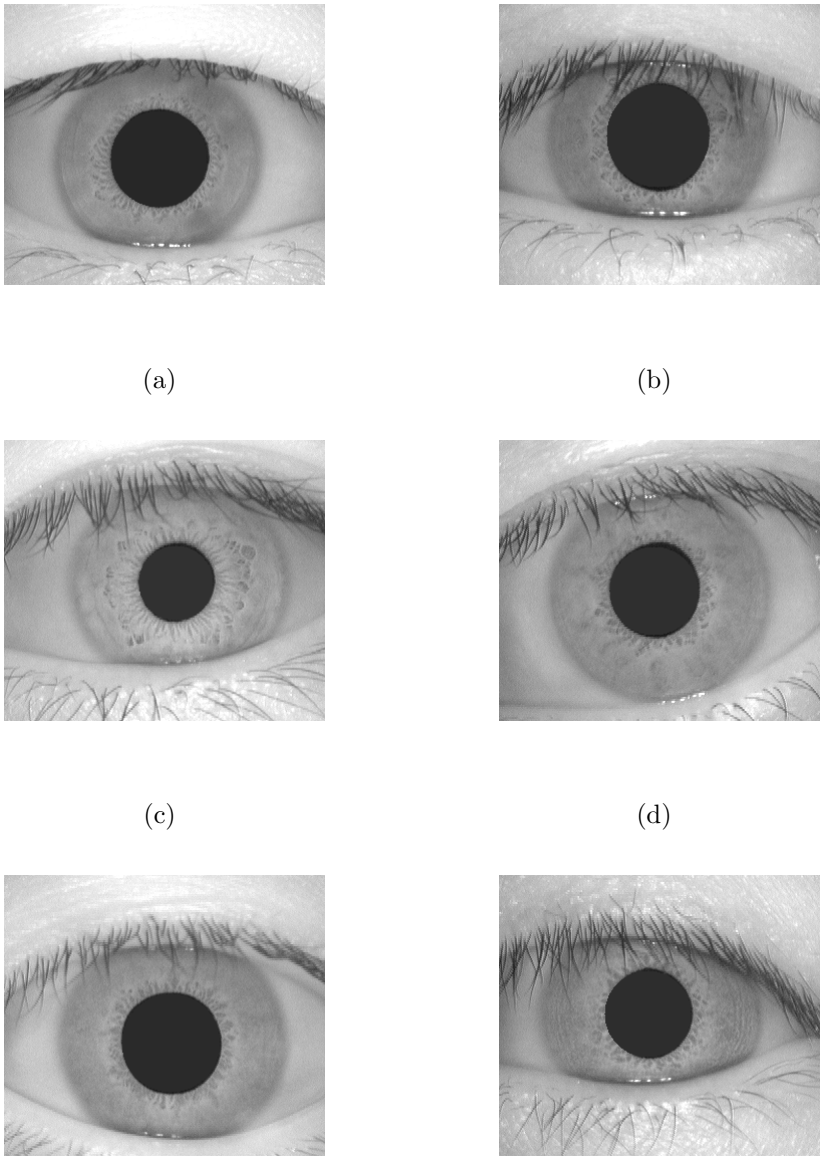

(a) (b)

(c) (d)

(e) (f)

Figure 4.11: (a)-(f) illustrate some eye images from CASIA database.

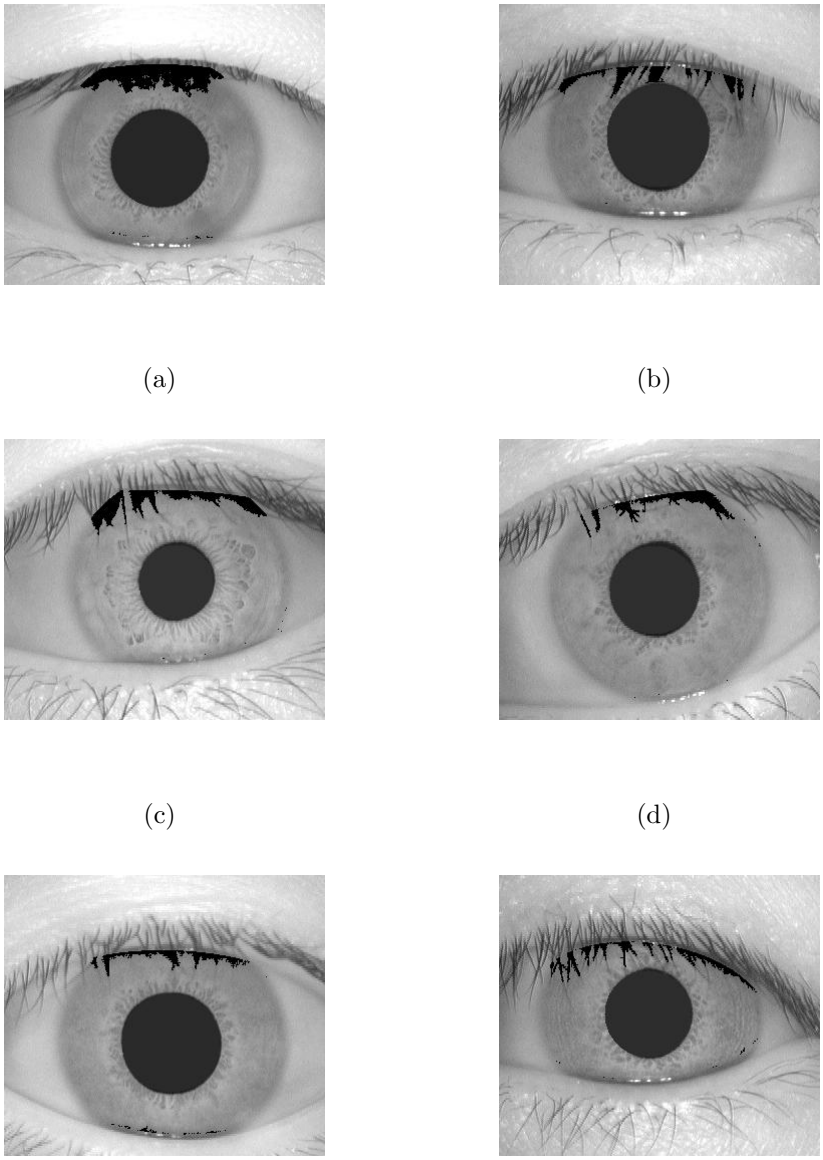

(a) (b)

(c) (d)

(e) (f)

Figure 4.12: (a)-(f) illustrate the results of the eyelash detection algorithm. The algorithm is based on MAP classification combined with a connectivity criterion. The connectivity criterion assumes that an eyelash pixel is either connected to another eyelash pixel or to the detected eyelid contours.

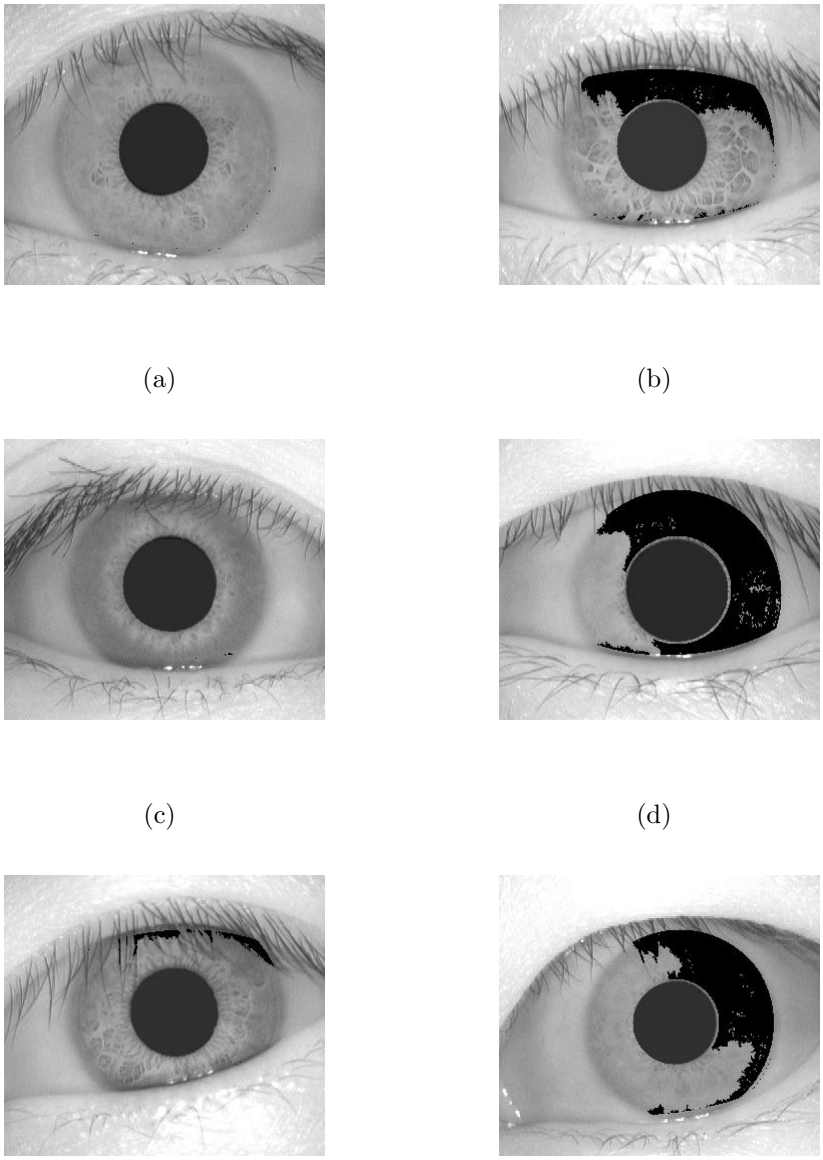

(a) (b)

(c) (d)

(e) (f)

Figure 4.13: Inaccurate eyelash detection. (a),(c),(e) illustrate the inaccurate results of the eyelash detection algorithm due to over estimating the MAP threshold. (b),(d),(f) illustrate the inaccurate results of the eyelash detection algorithm due to under estimating the MAP threshold.

4.2 Normalization

In the field of iris recognition, performance of most systems are compared to the algorithm proposed by Daugman, which is considered as the state-of-the-art in the field. A Daugman-like algorithm has been developed to test different methods of segmentation and normalization to better demonstrate their impact on the system. Because of the differences in the implementation of the algorithm and the different images used in our experiments compared to other works, the results are based on demonstrating improvements within the developed algorithm to present a fair comparison of various techniques. 424 properly localized iris images are used throughout all the experiments and the Daugman's feature extraction method, 2D Gabor filter, is used to create the iris templates.

In order to illustrate the effect of different normalization methods on performance of the system, the recognition results are examined. The developed 2D Gabor filter of the Daugman-like algorithm has been used and the decidability index, *d'*, of the methods are compared. The 2D Gabor filter is defined as:

$$h_{(Re,Im)} = sgn_{(Re,Im)} \int_{\rho} \int_{\phi} I(\rho,\phi) e^{-j\omega(\theta_0-\phi)} e^{-(r_0-\rho)^2/\alpha^2} e^{-(\theta_0-\phi)^2/\beta^2} \rho d\rho d\phi, \qquad (4.1)$$

where $I(\rho,\phi)$ is the raw iris image in the dimensionless polar coordinates. α and β are the multi-scale 2D wavelet size parameters and ω is the wavelet frequency. (r_0,θ_0) are the polar coordinates of each region of iris that the features are computed. The iris templates of our experiments are obtained by applying the Gabor filter in $8 \times 128 = 1024$ locations of the iris textures. The 8×128 indicates 8 radial locations and 128 angular locations and the templates are 2048 bits, where 2 bits are extracted from each location of iris due to the phase demodulation process.

The radial resolution of $I(\rho,\phi)$ and the value of α are fixed throughout all the experiments in order to reduce the number of changing parameters. The radial resolution of the polar images are fixed to 90 pixels, which is chosen based on an initial experiment. In this experiment, the *d'* index of different angular and radial resolutions are obtained over a smaller iris database. Using these values, two average *d'* graphs are obtained by averaging over the angular and radial resolutions. Figure 4.14 illustrates the average *d'* over the radial resolutions varying from 9 to 180 pixels with respect to angular resolution. Figure

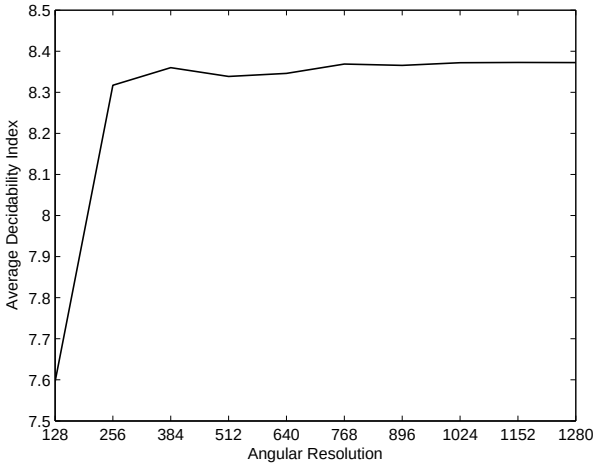

Figure 4.14: The average *d'* with respect to angular resolution for the fixed-size normalization method. As it is shown, increasing the angular resolution higher than 384 would not improve the normalization performance significantly.

4.15 illustrates the average *d'* over angular resolutions varying from 128 to 1280 pixels with respect to radial resolution. It is shown that the average *d'* would not vary much when the angular and radial resolutions become more than certain values. The angular resolutions more than 256 pixels and the radial resolutions more than 54 pixels result in *d'* values that would not change the *d'* significantly. Based on these results, a fixed radial resolution of 90 pixels, which is more than 54 pixels, is chosen for the experiments in order to reduce the number changing parameters.

4.2.1 Iris Unwrapping

In order to evaluate the presented unwrapping methods, *d'* is obtained with respect to different values of $\beta = (64, 48, 32, 24, 16)$. In this case, an angular resolution of 1280 pixels is chosen throughout the experiments, which is selected based on the average *d'* of figure 4.14.

Figure 4.16 demonstrates the results of an experiment where the unwrapping reference

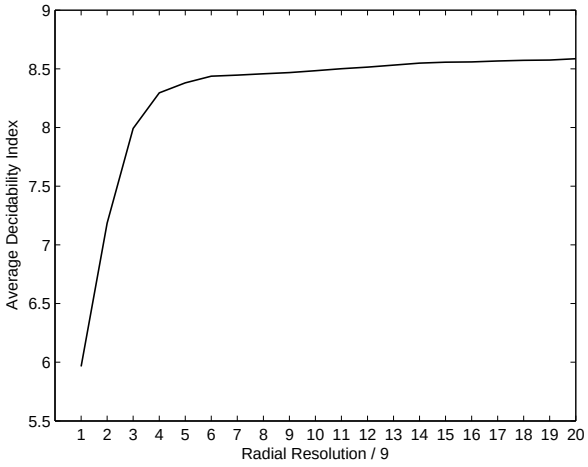

Figure 4.15: The average *d'* with respect to radial resolution for the fixed-size normalization method. As it is shown, increasing the radial resolution higher than 54 would not improve the normalization performance significantly.

point is linearly moving from limbus center to pupil center. The figure illustrates that recognition results constantly improve for all values of β when the reference point moves toward the pupil center. The results of this experiment have been the motivation to present the linearly-guessed reference point, which is the expected center of pupil when the pupil radius becomes zero. Figure 4.17 illustrates the results of the linearly-guessed method. The linearly-guessed reference point has improved *d'* significantly compared to the pupil and limbus centers.

Figure 4.18 is also the comparison of the linearly-guessed method with the two minimum distance unwrapping methods, where the linearly-guessed method illustrates better performance with respect to all values of β.

The linearly-guessed unwrapping method provides better recognition results compared to the other methods. It can be concluded that the method results in better alignment of iris textures. One of the weaknesses of previous segmentation approaches was the irregular shape of the pupil contours that can cause misalignments of iris textures. Considering a circular contour for the pupil borders that are not perfectly circular causes a misalignment

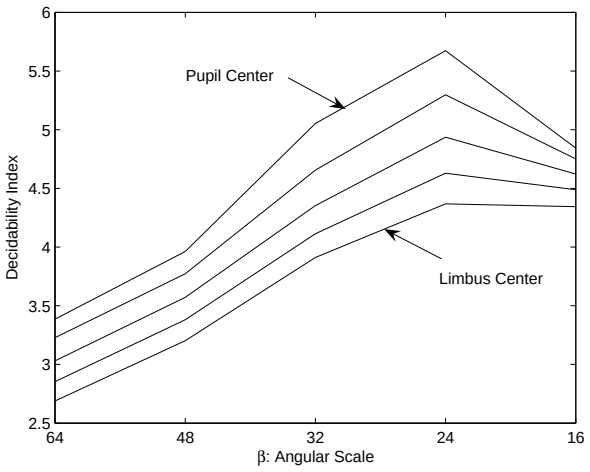

Figure 4.16: The recognition results from limbus center to pupil center. The recognition results constantly improve for all values of β when the reference point moves from limbus center toward pupil center.

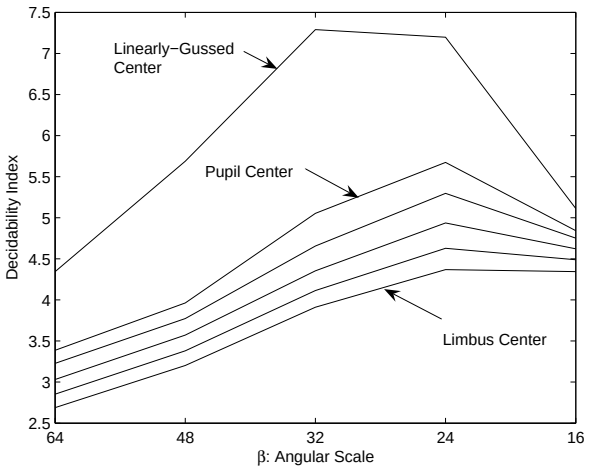

Figure 4.17: The comparison of the linearly-guessed center with limbus and pupil. The linearly-guessed center performs much better than the other reference points.

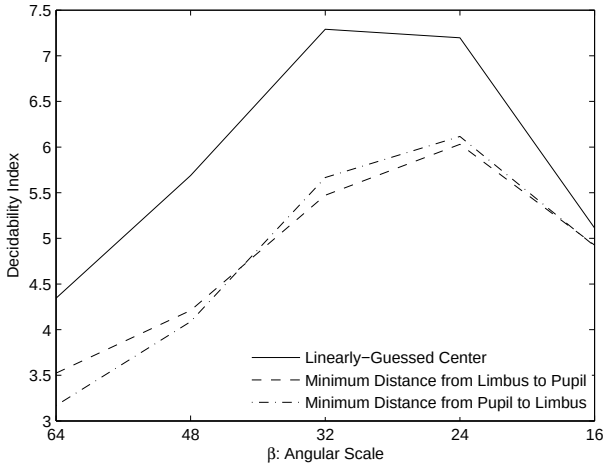

Figure 4.18: The comparison of the linearly-guessed center with the minimum distance methods. The linearly-guessed center performs much better than the minimum distance methods.

condition, specially in the radial direction. In order to illustrate the effect of the problem, an experiment has been done to compare the recognition results of three methods:

1. The linearly-guessed method using the circular pupil detection,
2. The linearly-guessed method using the proposed near-circular active contour,
3. The proposed contour-based method using the near-circular active contour.

Figure 4.19 illustrates performance of the three methods. It is shown that the recognition results of the linearly-guessed method is improved when the near-circular active contour is applied instead to the perfect circle. Moreover, the classification results are improved further when the contour-based method is applied instead of the linearly-guessed method. The contour-based method has shown to have more robustness compared to linearly-guessed method which is required to define the contour center point. Figure 4.20 illustrates the overall improvement of the contour-based method using the near-circular active contour compared to the linearly-guessed method using the circular contours. It

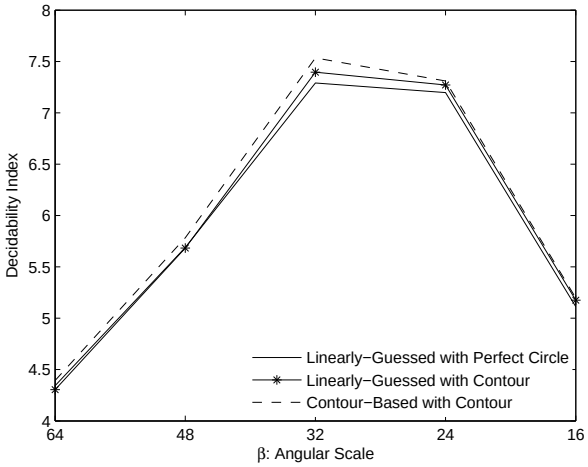

Figure 4.19: The impact of the active contour and the contour-based unwrapping method. This figure illustrates that the proposed active contour would improve the the recognition results compared to the circular pupil detection method. It is also demonstrated that the proposed contour-based method would further improve the performance compared to the linearly-guessed method.

should be mentioned that our experiments are designed to depict the improvements of the system regardless of the choice of parameters such as β. Therefore, the experiments are designed to test different values of β and illustrate the improvements in each choice of the parameter. The experiments demonstrate the improvement of the overall performance of the system with respect to different unwrapping methods.

4.2.2 Iris Normalization

Two different sampling approaches have been introduced: The commonly used fixed-size sampling and the proposed dynamic sampling. In order to evaluate and compare the two methods, the recognition results are obtained with respect to different values of $\beta = (48, 32, 24)$. It should be reminded that α and the radial resolution are fixed throughout the experiments. Therefore, in the main formulation of the Gabor filter, equation 4.1, the

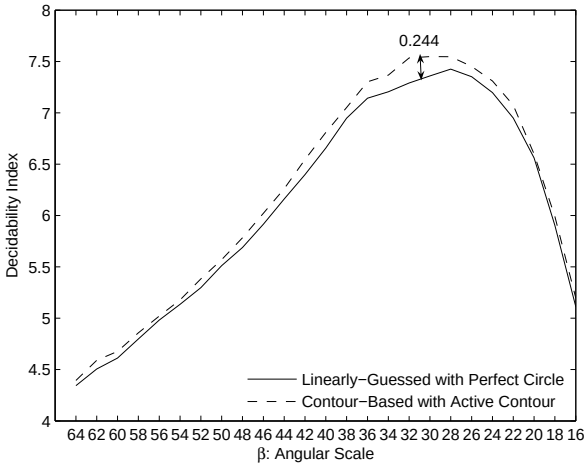

Figure 4.20: The overall improvement obtained by the contour-based method using the near-circular active contour compared to the linearly-guessed method using the circular pupil detection. In terms of *d'* index, the improvement is 0.244

only parameter that would change is the angular resolution of the polar image $I(\rho, \phi)$. The recognition results of different angular resolutions ranging from 128 to 1280 pixels are illustrated in figure 4.21. The figure shows the value of *d'* with respect to the three values of $\beta = (48, 32, 24)$ and the average value of the obtained *d'* indexes. In this graph, it can also be observed that the recognition results would not improve significantly when the angular resolution becomes greater than about 256 pixels.

The results of the proposed dynamic-size method are shown in figure 4.22 with the same values of β used for the fixed-size method. The angular resolution is obtained as $Resolution_{Angular} = 2\pi R \times K$. R refers to the radial location and it is defined in pixels. K is a factor intuitively chosen to vary from 0.3 to 1.2 which defines the sampling ratio with respect to the perimeter of the radial location. It is shown in this figure that the average recognition results would become stable for values of K greater than 0.5. This could be the interpreted as the effect of existing textural correlation of irises, which causes the sampling ratios lower than 1 to have the same recognition results as the sampling ratios larger than 1. Similar results were obtained in the fixed-size sampling method, where the resolutions

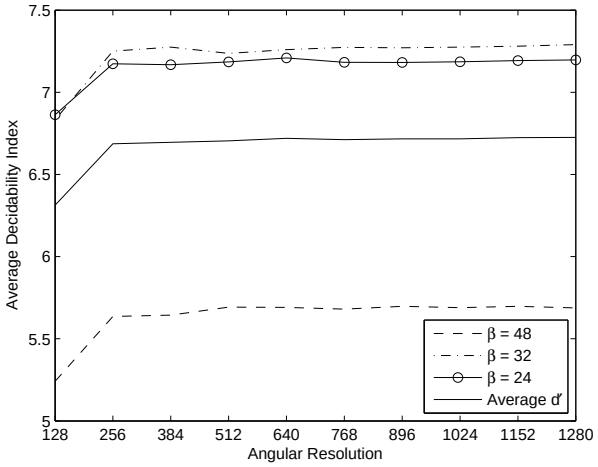

Figure 4.21: The recognition results of the fixed-size normalization method

greater than 256 pixels would result in the same values of *d'*. An angular resolution of 256 results in loss of information in the areas close to limbus where the number of pixels are more.

Figure 4.23 is a comparison of the average decidability indexes obtained by the two methods. It should be mentioned that the horizontal axis which indicates the angular resolution is different for the two methods. The fixed resolution is defined from 128 to 1280 pixels and the dynamic resolution varies by the ratio factor K from 0.3 to 1.2. The two graphs are plotted in the same space in order to better illustrate the recognition results. As it is shown in this figure, the values of *d'* for the dynamic sampling method is higher than the fixed method. The maximum value of the average *d'* of the dynamic sampling is equal to 6.803, while the maximum value of the fixed sampling is equal to 6.719. The difference of their *d'* index is 0.084.

4.3 Summary

In this chapter, we have examined the proposed methods presented in chapter 3. The experimental results show that the proposed near-circular active contour can accurately

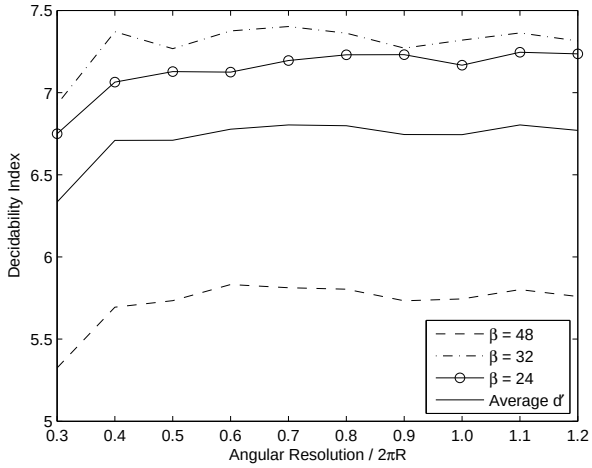

Figure 4.22: The recogniton results of the dynamic-size normalization method

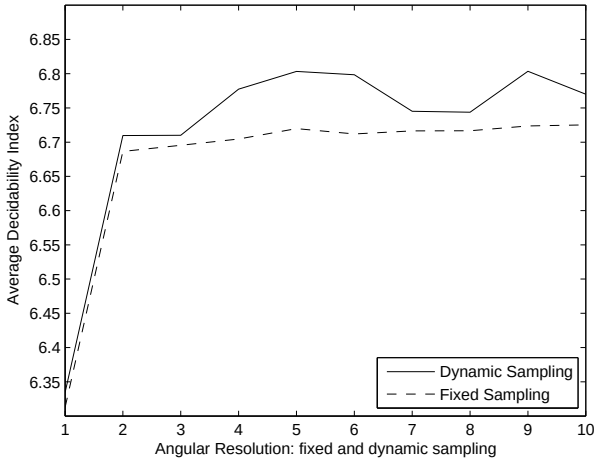

Figure 4.23: The comparison of the average *d'* of dynamic and fixed methods. It is shown that the dynamic normalization method improves the recognition performance compared to the fixed-size method.

detect all the pupil boundaries in the CASIA database. They also indicate that combining the near-circular active contour and the contour-based normalization method can effectively enhance the performance. In terms of *d'* index, the improvement is 0.244. Comparing several normalization methods, our experiments pinpoint that the contour-based method provides the best performance. We also compare the dynamic-size and fixed-size normalization approaches. This comparison shows that the dynamic method is slightly more accurate than the fixed-size method. The difference of their *d'* index is 0.084.

Chapter 5

Conclusions

This thesis is to enhance the performance of segmentation and normalization processes in iris recognition systems to increase the overall accuracy. A Daugman-like algorithm was developed in order to evaluate the impact of different segmentation and normalization methods on the overall performance. 424 properly localized iris images were used in all the experiments and 2D Gabor filter was used to create iris templates.

Properly detecting the inner and outer boundaries of iris texture is important for all iris recognition systems. The irregular boundary of pupil was the motivation of designing an active contour for detecting the boundary accurately. The active contour takes into consideration that an actual pupil boundary is a near-circular contour rather than a perfect circle. This method successfully detects all the pupil boundaries in the CASIA database and improves the recognition results.

Transforming iris texture into polar coordinates requires a proper reference point as the origin. The performance of limbus center, pupil center and the linearly-guessed center are examined. The experiments demonstrate that the linearly-guessed center improves the recognition accuracy significantly. Moreover, more improvements are achieved from a new contour-based normalization method, which is based on reformulating the normalization problem as a minimization problem. In terms of *d'* index, the improvement obtained by the contour-based method compared to the linearly-guessed method is 0.244.

In addition, previous normalization methods are based on transforming iris texture into a fixed-size rectangular block. However, the size parameter of normalized iris has not been

investigated in details. According to our experiments, the optimal parameter for fixed-size rectangular shape is 54×384. Further increasing the size of the rectangle would not improve the normalization performance significantly. In addition to evaluating the fixed-size approach, a dynamic normalization method is proposed. Experimental results show that the dynamic method can improve the recognition performance. In terms of d' index, the improvement is 0.084.

Bibliography

[1] F. H. Adler, "hysiology of the Eye." *St. Louis, MO: Mosby, 1965.*

[2] A. Bertillon, "a couleur de liris." *Rev. Sci., vol. 36, no. 3, pp. 6573, 1885.*

[3] L. Flom and A. Safir, "ris recognition system." *U.S. Patent 4 641 349, 1987.*

[4] Obaidat, M.S., Sadoun, B.: "Verification of computer users using keystroke dynamics." *IEEE Transactions on Systems, Man and Cybernetics 27 (1997) 261269.*

[5] C. Shannon and W. Weaver, "he Mathematical Theory of Communication." *U. Illinois Press, Urbana, Ill., 1949.*

[6] J.G Daugman. "ris recognition." *American Scientist, July-Aug. 2001.*

[7] J.G Daugman, "High Confidence Visual Recognition of Persons by a Test of Statistical Independence." *IEEE Transactions On Pattern Analysis and Machine Intelligence, Vol. 15, No.11, pp.1148-1161,Nov. 1993.*

[8] J.G Daugman. "How iris recognition works." *Proceedings of 2002 International Conference on Image Processing, Vol. 1, 2002.*

[9] J.G Daugman, "The importance of being random: Statistical principles of iris recognition." *in Pattern Recognition, Vol. 36, No. 2, pp. 279–291, 2003.*

[10] J.G Daugman, "Demodulation by Complex-Valued Wavelets for Stochastic Pattern Recognition." *Int'l J. Wavelets, Multiresolution and Information Processing, vol. 1, no. 1, pp. 1-17, 2003.*

[11] R. Wildes, J.C. Asmuth, G.L. Green, S.C. Hsu, R.J. Kolczynski, J.R. Matey and S.E. McBride, "A system for automated iris recognition." *In Proceedings of the IEEE Workshop on Applications of Computer Vision, pp. 121-128, 1994.*

[12] R. Wildes J. Asmuth G. Green S. Hsu R. Kolczynski J. Matey and S. McBride, "A Machine-Vision System for Iris Recognition." *Machine Vision and Applications, vol. 9, pp. 1-8, 1996.*

[13] R. Wildes, "Iris Recognition: an Emerging Biometric Technology." *Proceeding of the IEEE, Vol. 85, No. 9, 1997.*

[14] W.W. Boles, "A wavelet transform based technique for the recognition of the human iris." *In Proceedings of the International Symposium on Signal Processing and its Application, ISSPA, Gold Coast, Australia, pp. 25-30, August, 1996.*

[15] W.W. Boles and B. Boashash, "A human identification technique using images of the iris and wavelet transform." *IEEE Transactions on Signal Processing, vol. 46, no. 4, pp. 1185-1188, 1998.*

[16] C. Tisse L. Martin L. Torres and M. Robert, "Person Identification Technique Using Human Iris Recognition." *Proc. Vision Interface, pp. 294-299, 2002.*

[17] Y. Zhu, T. Tan and Y. Wang "Biometric personal identification based on iris pattern." *Proceeding of. 15th International Conference on Pattern Recognition, vol. 2, pp. 801-804, 2000.*

[18] S. Lim K. Lee O. Byeon and T. Kim, "Efficient Iris Recognition through Improvement of Feature Vector and Classifier." *ETRI J., vol. 23, no. 2, pp. 61-70, 2001.*

[19] S. Noh, K. Pae, C. Lee, J. Kim. "Multiresolution independent component analysis for iris identification." *The 2002 International Technical Conference on Circuits/Systems, Computers and Communications, Phuket, Thailand, 2002.*

[20] L. Ma, Y. Wang, T. Tan. "Iris recognition using circular symmetric filters." *National Laboratory of Pattern Recognition, Institute of Automation, Chinese Academy of Sciences, 2002.*

[21] C. Seal, M. Gifford and D. McCartney, "Iris recognition for user validation." *British Telecommunications Engineering Journal, vol. 16, pp. 113-117, July 1997.*

[22] M. Negin, T.A. Jr, M. Salganicoff, T.A. Camus, U.M. von Seelen, P.L. Venetianer and G.G. Zhang, "An iris biometric system for public and personal use." *Computer, vol. 33, no. 2 , pp. 70-75, 2000.*

[23] G.O. Williams, "Iris recognition." *IEEE Aerospace and Electronics Systems Magazine, vol.12, no. 4, pp. 23-29, April 1997.*

[24] K. Hanna, R. Mandelbaum, L. Wixson, D. Mishra, and V. Paragana, "A system for nonintrusive human iris acquisition." *In Proc. Int. Association for Pattern Recognition Workshop on Machine Vision Applications, Tokyo, Japan, 1996, pp. 200203.*

[25] W. Ketchantang, S. Derrode, S. Bourennane, L. Martin, " Video Pupil Tracking for Iris Based Identification." *In proceeding of 7th International Conference on Advanced Concepts for Intelligent Vision Systems, ACIVS 2005, Antwerp, Belgium, September 20-23, 2005.*

[26] Kang Ryoung Park, Jaihie Kim: "A real-time focusing algorithm for iris recognition camera." *IEEE Transactions on Systems, Man, and Cybernetics, Part C 35(3): 441-444 (2005).*

[27] Bressloff, P.C., Wood, C.V. and Howarth, P.A. (1996). "Nonlinear shunting model of the Pupil Light Reflex." *Proc. Royal Soc. B, vol. 263, pp. 953-960.*

[28] X. Xie, R. Sudhakar, and H. Zhuang, "Real-time eye feature tracking from a video image sequence using kalman filter." *IEEE Transactions on Systems, Man and Cybernetics, vol. 25, no. 12, pp. 1568-1577, 1995.*

[29] J. Huang, Y. Wang, T. Tan, Jiali Cui, "A new iris segmentation method for recognition." *In Proceedings of the 17th International Conference on Pattern Recognition, ICPR, Volume: 3, pp. 554- 557 Vol.3 2004.*

[30] W. Kong, D. Zhang. "Accurate iris segmentation based on novel reflection and eyelash detection model." *Proceedings of 2001 International Symposium on Intelligent Multimedia, Video and Speech Processing, Hong Kong, 2001.*

[31] W. K. Kong and D. Zhang, "Eyelash detection model for accurate iris segmentation." *in Proceeding of ISCA 16th International Conference on Computers and their Applications, March 28-30,2001, pp. 204-207, Seattle, Washington, USA.*

[32] B. J. Joung, J. O. Kim, C. H. Chung, Key Seo Lee, Wha Young Yim, Sang Hyo Lee, " On Improvement for Normalizing Iris Region for a Ubiquitous Computing." *In Proceedings of International Conference on Computational Science and Its Applications ICCSA 2005, Singapore, May 9-12, 2005.*

[33] X. Yuan, P. Shi, "A Non-linear Normalization Model for Iris Recognition." *In Proceedings of International Wokshop on Biometric Recognition Systems on Advances in Biometric Person Authentication, IWBRS 2005, Beijing, China, October 22-23, 2005.*

[34] Harry J. Wyatt: "A Minimum-wear-and-tear Meshwork for the Iris." *In: Vision Research. 40 (2000) 2167-2176*

[35] N. Ritter, "Location of the Pupil-Iris Border in Slit-Lamp Images of the Cornea." *Proceedings of the international Conference on Image Analysis and Processing, 1999.*

[36] N. J. Ritter and J. R. Cooper, "Locating the iris: A first step to registration and identification." *in Proc. 9th IASTED International Conference on Signal and Image Processing, pp. 507-512, IASTED, Aug. 2003.*

[37] M. Kass, A. Witkin, D. Terzopoulos. Snakes: "Active Contour Models." *International Journal of Computer Vision, 1987.*

[38] S. Lobregt and M. A. Viergever, "A Discrete dynamic contour model." *IEEE Transactions on Medival Imaging, 14(1), 1995, 12-24.*

[39] N. Wiener, "Times Series." *Cambridge, MA: M.I.T. Press, 1949.*

[40] J.P.Havlicek, J.W.Havlicek and A.C.bovik, "the analytic image." *IEEE Journal, 1997.*

[41] J. R. Bergen, P. Anandan, K. Hanna, and R. Hingorani, "Hierarchical model-based motion estimation." *in Proc. Euro. Conf. Computer Vision, Santa Margherita Ligure, Italy, 1991, pp. 510.*

[42] *Chinese Academy of Sciences Institute of Automation.* Database of 756 Greyscale Eye Images. page http://www.sinobiometrics.com.

[43] *International Biometrics Group* page http://www.biometricgroup.com/.

[44] *UK Passport Service* page http://www.passport.gov.uk/index.asp.

[45] *US Department of Homeland Security* page http://www.dhs.gov/dhspublic/.